IDŐJÁRÁS

QUARTERLY JOURNAL
OF THE HUNGARIAN METEOROLOGICAL SERVICE

CONTENTS

VOL. 97 * NO. 4 * OCTOBER–DECEMBER 1993

IDŐJÁRÁS

Quarterly Journal of the Hungarian Meteorological Service

Editorial Office: P.O. Box 39, H–1675 Budapest

Subscription from customers in Hungary should be sent to the Financial Department of the Hungarian Meteorological Service Kitaibel Pál u. 1, 1024 Budapest. The subscription rate is HUF 2000.

Abroad the journal can be purchased from the distributor: KULTURA, P.O. Box 149, H–1389 Budapest. The annual subscription rate is USD 56.

IDŐJÁRÁS

Quarterly Journal of the Hungarian Meteorological Service
Vol. 97, No. 4, October–December 1993

Forward trajectory calculation program system for the Central European region

Z. Ferenczi and **K. Labancz**

Institute for Atmospheric Physics,
P.O. Box 39, H-1675 Budapest, Hungary

(Manuscript received 4 October 1993; in final form 22 November 1993)

Abstract – A program system for predicting wind fields and air parcel trajectories at the 850 hPa pressure level is described. The computer model calculates the possible path of a radioactively polluted air parcel started in any accidental event at a nuclear power station in the Central European region. A case study for Paks, Hungary on 26 August 1993 is presented.

Key-words: transport of air pollutants, wind field calculation, air trajectories.

1. Introduction

The environmental impact of the transport of atmospheric pollutants such as chemical components as well as radioactive elements from an isolated source has become increasingly important in recent years. The claim to predict the trajectories of air masses transporting radioactive or chemical pollutants came to the front after several accidents in nuclear power plants.

A forward trajectory calculation program system is being developed at the Hungarian Meteorological Service for predicting wind at the 850 hPa pressure level and air parcel trajectories for one day over the Central European region.

The program system consists of two main parts: the first part produces a mesoscale wind field, the other calculates trajectories over this field. Because we have limited computer resources and sparse spatial resolution of measured input data, only a simplified model for diagnosing and forecasting the wind field could be chosen. We examined three kind of simplified models: a mass conversation model (*Dickerson*, 1978) which was not expected to function well in a region with sparse data, a one-layer vertically integrated primitive equation model introduced by *Lavoie* (1974) which was suspectible to numerical instability, and a one-level version of the primitive equations in sigma-coordinates

first developed by *Danard* (1977). This model integrates tendency equations for pressure, potential temperature and wind only at the surface and does not demand mass conservation. A version of the Danard model—called MESMOD model—was refined and further developed by *Mass* and *Dempsey* (1985) at the University of Washington. The qualitative stability investigation of their model was done by *Barát* (1990) at the Eötvös Loránd University, Budapest. In according to this investigation the MESMOD model has the potential for diagnosing the important details of the low level wind field and it is computationally stable and efficient.

For computing the air parcel trajectories the kinematic method of *Petterssen* (1956) has been chosen. As a widely used transport level, the 850 hPa pressure level was selected for the calculations. At this pressure level we forecast the wind field for one day by the modified MESMOD model and then we calculate the trajectories.

2. *Calculation of the wind field*

2.1 MESMOD—the mesoscale model for diagnosing surface winds

The original model (MESMOD—*Mass* and *Dempsey*, 1985) is suitable for diagnosing surface winds. The model has been modified for predicting winds at the 850 hPa pressure level for one day.

The original MESMOD is a single-layer, sigma-coordinate, mesoscale model. The basic equations of the model are the horizontal momentum equations and the first law of thermodynamics; these are given in sigma-coordinates at the surface

$$\frac{\partial \vec{v}_s}{\partial t} = -\vec{v}_s \nabla_\sigma \vec{v}_s - f\vec{k} \times \vec{v}_s - (g\nabla_\sigma z_s + RT_s \nabla_\sigma \ln p_s) + \vec{F} + K_M \nabla_\sigma^2 \vec{v}_s, \quad (1)$$

$$\frac{\partial T_s}{\partial t} = -\vec{v}_s \nabla_\sigma T_s + \frac{RT_s}{c_p}\left(\frac{\partial \ln p_s}{\partial t} + \vec{v}_s \nabla_\sigma \ln p_s\right) + \frac{Q}{c_p} + K_T \nabla_H^2 T, \quad (2)$$

where $\vec{v}_s$, T_s, p_s are wind vector, temperature and pressure, respectively, at the surface, z_s is the height of the surface. f denotes the Coriolis parameter, g the gravitational acceleration, c_p the specific heat capacity, and $\vec{F}$ is the frictional force. K_M and K_T represent the momentum and the temperature horizontal diffusion, and finally Q is the diabatic heating. For the deduction of equations $\dot{\sigma}=0$ at surface level was applied.

The third unknown variable in the equations is the surface pressure. This variable is a diagnostic one, because it does not have tendency in Eqs. (1) and (2).

p_s can be determined by integrating the hydrostatic equation between the surface and the 850 hPa pressure level. To this end we suppose that the pollution processes are taking place between the surface and the 850 hPa pressure level, at which the geopotential height and temperature fields are known. Furthermore, we assume that the topographically caused orographic flow occurs within a 2 km layer above the surface.

The prognostic variables of the model are $\vec{v}_s$ and T_s. T_s refers to the surface layer. The values of the wind speed calculated by the model are related to the upper boundary of the friction layer, 50–100 m height. In vertical direction linear thermal stratification is assumed in the model.

The diabatic effect depends on the daily variation of the radiant exposure, the frictional force can be expressed as the vertical divergence of the stress, the horizontal diffusion of the momentum and the temperature are parameterized in the model.

2.2 The wind field at the 850 hPa pressure level

For calculating the path of radioactive elements over a region, the 850 hPa pressure level is widely used. Therefore the previously described model has been re-written for predicting winds at the 850 hPa pressure level.

The coordinate system used is a σ-system

$$\sigma = \frac{p - 850}{p_s - 850}.$$

The choice of the σ-system is reasonable because at the surface $\sigma = 1$ and at the 850 hPa pressure level $\sigma = 0$, hence $\dot{\sigma} = 0$ (*Práger*, 1982). Substituting this expression into the momentum and temperature tendency equations we obtain the following equations

$$\frac{\partial \vec{v}_{850}}{\partial t} = -\vec{v}_{850} \nabla_\sigma \vec{v}_{850} - f\vec{k} \times \vec{v}_{850} - g \nabla_\sigma z_{850} + \vec{F} + K_M \nabla_\sigma^2 \vec{v}_{850}, \qquad (3)$$

$$\frac{\partial T_{850}}{\partial t} = -\vec{v}_{850} \nabla_\sigma T_{850} + \frac{R T_{850}}{c_p} \left(\frac{\partial u_{850}}{\partial x} + \frac{\partial v_{850}}{\partial y} \right) + \frac{Q}{c_p} + K_T \nabla_\sigma^2 T_{850}. \qquad (4)$$

In these equations we apply the earlier notations, $\vec{v}_{850}$ and T_{850} denote the 850 hPa pressure level wind vector and temperature, respectively. By the production of this motion field we parameterize the diabatic warming and cooling, the horizontal diffusion as well as the frictional force.

3. *Calculating kinematic trajectories*

It is well known that the trajectories indicate the actual path which an air parcel travels along. *Ihász* (1992) investigated the different trajectory calculation methods used in meteorological practice. In our program system we use an isobaric method for the 850 hPa level.

If the $\vec{v}(x,y,z,t)$ wind field and its temporal variation are known, the trajectory of a parcel situated at the point $\vec{r}_o(x_o,y_o,z_o)$ and at the moment $t=t_o$ can be determined as the solution of the initial value problem referring to the differential equation defining the wind field

$$\vec{r}(t) = \vec{r}_o(t_o) + \int_{t_o}^{t} \vec{v}(\vec{r}(\tau))d\tau . \tag{5}$$

As an approach of this integration formula we use the kinematic iterative method suggested by *Petterssen* (1956). The $\vec{v}(\vec{r}(t))$ wind field at the 850 hPa pressure level in the form of successive wind charts for 24 hours is available as the result of the MESMOD model. After a given Δt time step, the new position of an air parcel started from $\vec{r}_o$ point is calculated by means of the following iterational steps:

(1) We draw the $\delta\vec{r}_1=\vec{v}(\vec{r}_o(t_o))\Delta t$ displacement vector. Thus on the next map the parcel would arrive at the point Q_1 (see *Fig. 1*).

(2) In the meantime the pressure distribution has changed so we have to draw the $\delta\vec{r}_2=\vec{v}(\vec{r}_o+\delta\vec{r}_1(t_o+\Delta t))\Delta t$ displacement vector.

(3) As a second approximation of the new position of the air parcel we draw the displacement vector $\delta\vec{r}_1=\frac{1}{2}(\delta\vec{r}_1+\delta\vec{r}_2)$ and the point Q_2.

(4) The operation described in the 2nd and 3rd steps should be repeated until the difference between $\delta\vec{r}^{(n-1)}$ and $\delta\vec{r}^{(n)}$ will be small enough. Δt and n were set to 1 hour and 2, respectively. This method is shown in Fig. 1.

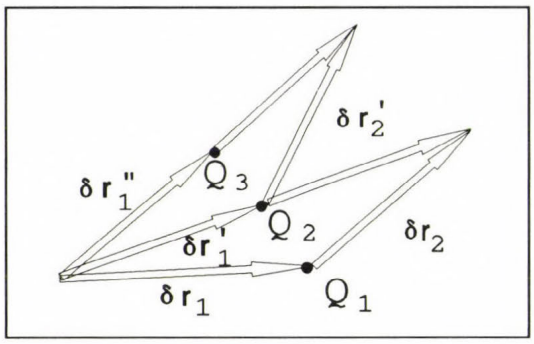

Fig. 1. Scheme for the use of the trajectory method.

4. The data base used

The area to be investigated is located between 12.5°E–25°E and 40°N–50°N. The grid resolution of the used terrain field is 1/3° along both longitude and latitude, which gives 30×38 grid points over the area.

As initial conditions the program needs temperature and geopotential height at the 850 hPa level at the initial moment of the model integration. The so called GRID data from the British Meteorological Office (Bracknell) have been used for this purpose. The resolution of the GRID information is 2.5°×2.5°, so there are 5×6 GRID points in the domain of the MESMOD model. For interpolating the GRID data over the model area the formula

$$\varphi = \frac{\sum_i \left(\frac{\varphi_i}{r_i^2} \right)}{\sum_i \left(\frac{1}{r_i^2} \right)} \tag{6}$$

is used, where φ is any variable in the grid point of MESMOD, r_i is the distance between the grid point of MESMOD and the grid point of GRID, and φ_i is the given variable in the GRID.

5. Practical realization and results

First we have to produce the wind field over the area of our examination for calculating the trajectory with the required temporal resolution. The investigated area is Central Europe in the operational application. In this area we have to determine the wind field with hourly resolution in the next 24 hours.

After initialization, the model is integrated without diabatic heating to steady-state. After that the calculation of the wind field begins. The model makes an output at every Δt time step (in our examination Δt is equal to 1 hour). After producing the successive wind fields, the model starts to calculate the trajectories of the pollutants originating from a given point of the region.

The mesoscale model we use to calculate the wind field gives different results in different synoptic situations. In their paper the authors (*Mass* and *Dempsey*, 1985) mention that "There are situations in which this simple model is not suitable for diagnosing the low level wind field such as for high Froude number cases, ... e.g. during a frontal passage.". After some model runs for real cases we realised that except the above mentioned situations the model calculates the mesoscale wind field suitably but it gives only small changes in the predicted field, therefore it does not follow the quick meteorological changes such as frontal passages.

As an example we have chosen a calm meteorological situation on 26 August 1993 when a slowly moving cold front situated south of Hungary. To the north of the front there was a cold air mass over Europe and this situation had not considerably changed during that day. We calculated a trajectory of an imagined radioactively polluted air parcel started from the nuclear power station at Paks at 00 UTC on 26 August 1993. *Fig. 2* shows the wind field at the 850 hPa pressure level after one-hour integrating.

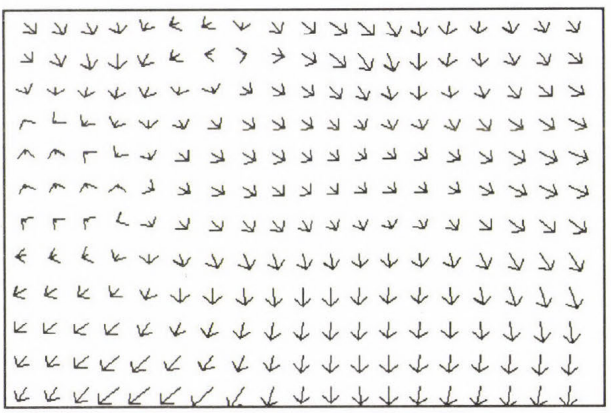

Fig. 2. The calculated wind field at the 850 hPa pressure level at 01 UTC on 26 August 1993 over the examined region.

The wind field had not changed on that day thus after 24 hours we could draw a trajectory started from Paks shown by *Fig.3.*

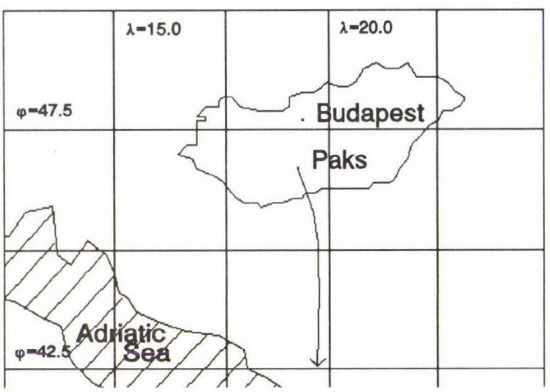

Fig. 3. Trajectory starting from Paks on 26 August 1993.

In the future we want to use this technique for forecasting the path of the air masses containing radioactive or chemical pollutants released in any

accident. For this purpose we intend to develop the capability of the mesoscale model to give better predictions of changing meteorological situations.

Acknowledgements—The authors are much indebted to *Dr. Tamás Práger* for valuable suggestions and comments.

References

Barát, I., 1990: *Qualitative Investigation of a Mesoscale Model Predicting Surface Air Flow* (in Hungarian). Master's Thesis.

Danard, M., 1977: A simple model for mesoscale effects of topography on surface winds. *Mon. Wea. Rev. 105*, 572-581.

Dickerson, M.H., 1978: MASCON–A mass consistent atmospheric flux model for regions with complex terrain. *J. Appl. Meteor. 17*, 241-253.

Ihász, I., 1992: Isobaric and isentropic objective analysis of meteorological fields for regional and continental scale trajectories. *Időjárás 96*, 81-92.

Lavoie, R.L., 1974: A numerical model of trade wind weather on Oahu. *Mon. Wea. Rev. 102*, 630-637.

Mass, C.F. and *Dempsey, D.P.*, 1985: A one-level, mesoscale model for diagnosing surface winds in mountains and coastal region. *Mon. Wea. Rev. 113*, 1211-1227.

Petterssen, S., 1956: *Weather Analyses and Forecasting*. Vol. I. McGraw-Hill, New York, Toronto, London.

Práger, T., 1982: *Numerical Prediction*. Part I. Lecture Notes (in Hungarian). Eötvös Loránd University, Budapest.

IDŐJÁRÁS

Quarterly Journal of the Hungarian Meteorological Service
Vol. 97, No. 4, October–December 1993

Comprehensive hydrostatic quality control of radiosonde height and temperature data

É. Borbás

Satellite Research Laboratory, Hungarian Meteorological Service,
P.O. Box 32, H-1675 Budapest, Hungary

(Manuscript received 13 August 1993; in final form 10 November 1993)

Abstract—The errors in observational data can damage analysis and forecast fields, so any control procedure of radiosonde data of height and temperature at the mandatory isobaric surfaces plays an important role in *numerical weather prediction* (NWP). We have created a hydrostatic quality control for the Hungarian NWP model. To this end we have chosen a *comprehensive hydrostatic quality control* (CHQC) method. The introduction gives a brief description of the history of *quality controls* (QC) and an experiment is presented to illustrate the effect of the erroneous data on the objective analysis. In the next two sections the method of CHQC is described. In the fourth section, a few examples show the efficiency of the method for different error types. At the end of the paper, we refer to statistical results, and conclusions and plans for the future are given.

Key-words: complex quality control, comprehensive hydrostatic quality control, decision-making algorithm.

1. Introduction

Meteorological observational data contain errors in a smaller or higher degree. These errors can be divided into two categories: the first one contains errors which have no large absolute values and they are inherent in all data. The second category of errors—*gross errors*—is the one which is important for us in this paper. They are caused by the failure of measuring instruments and/or by mistakes during data processing, transmission and reception. Gross errors can be very large, though they occur rarely. These errors are important because they can highly damage the analysis and forecast fields. In order to avoid them, it is necessary to control the meteorological information.

The Hungarian NWP model uses SYNOP and TEMP data over the European area. We have controlled the data of mandatory pressure levels of TEMP reports with the method which was designed and implemented at the

National Meteorological Center (NMC) in Washington, D. C. (*Gandin* and *Collins*, 1990). Two sets of observational data are available for our model: measured data at 00 and 12 UTC.

We have carried out an experiment in order to investigate the effect of the wrong data on analysis fields. First of all we have created a correct set of reports (12 UTC, 18th May 1993.). In *Fig. 1a* the objective analysis for these data can be seen. Afterwards we have artificially introduced stations with erroneous reports: we have damaged the height data of some selected stations [Bodø (01152), Vienna (11052), Budapest (12843) and Szeged (12982)] at 500 hPa with about 150–200 m. *Fig. 1b* shows the modified objective analysis field. The effect of these artificially introduced gross errors is significant, as it can be seen from the difference field of the two analyses for two damaged areas (*Fig. 1c, d*). Finally, we have corrected the wrong data with our method. The correction perfectly reproduced the original field. This experiment also proved the necessity of checking the observational data.

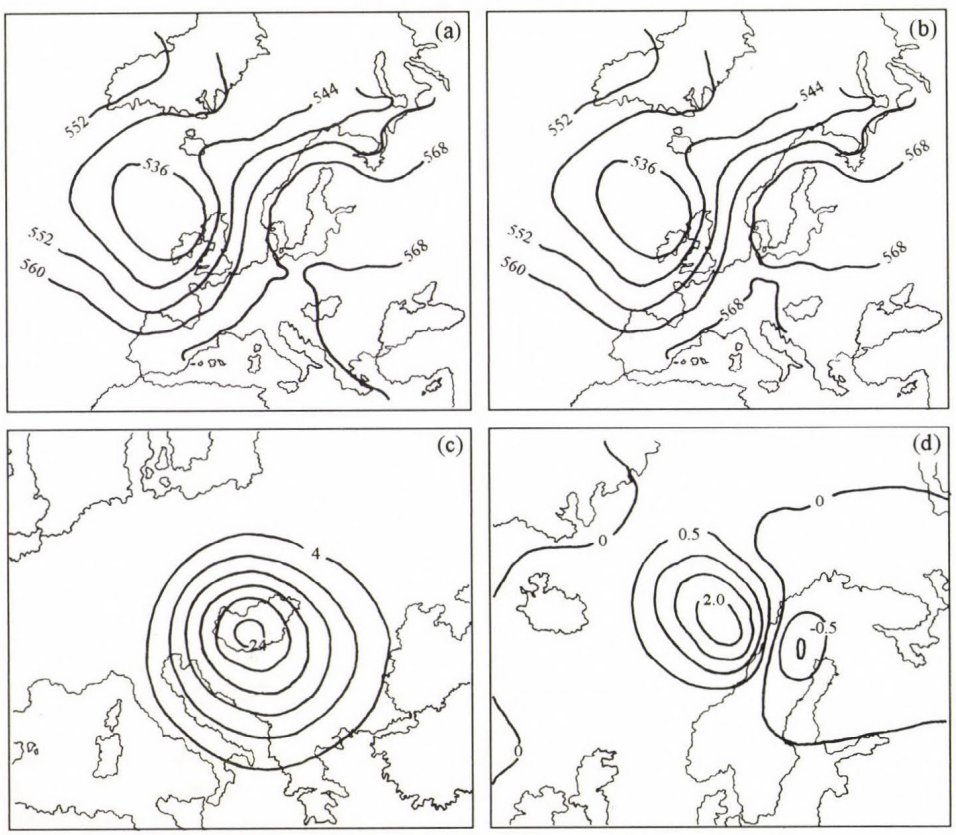

Fig. 1. 00 UTC 18th May 1993 analysis of 500 hPa geopotential height with correct data (*a*), and with erroneous data in some places (*b*) (values are given in dkm), difference fields for two erroneous areas (*c, d*).

The development of quality control (QC) of meteorological data is a sequence of actions directed against gross errors. The presence and danger of gross errors in meteorological data had been recognized before NWP activity was started. Visual examination of weather charts and other graphical representations were the only ways to detect these errors, so correction or rejection of erroneous data was done on the basis of subjective decisions. This manual QC was applied at the very beginning of the NWP era. At the dawn of NWP, the QC of meteorological information became much more important and its importance has permanently grown together with the improvement of analysis and NWP models. In this respect, we have to underline that the more improved a NWP model is, the more sensitive it is to the errors of initial data. Simultaneously, the problem of automatic QC has become much more complicated because of two factors: dramatic increase of the number of available meteorological data, and development and application of new meteorological observations. QC could not be accomplished manually because of the increasing number of meteorological data.

Several QC methods have been developed parallelly. The first objective analysis system was developed by *Gilchrist* and *Cressman* (1954) which contained an automatic QC. *Bergthorson* and *Döös* (1955) suggested the application of the first guess fields in objective analysis in order to check the observation data. The first version of hydrostatic check was suggested at the same time. *Belousov et al.* (1968) proposed the first version of the spatial continuity check in his three-level quasi-geostrophic NWP model. The next very important step in the QC development was the introduction of methods based on optimum interpolation. These were first developed in the USSR in the sixties. The multivariate three dimensional version of these methods was applied in 1977 (*Lorenc et al.*, 1977).

For a long time, however, QC was considered as a purely technical task. Fortunately, the situation has changed recently. Several QC methods are now being used sequentially and each of these made the decisions independently (*ECMWF*, 1985). The idea of *complex quality control* (CQC) was formulated by *Gandin* (1969). CQC is able to do more than horizontal and hydrostatical checks, as two QC methods are used sequentially: CQC is a more complex approach. The first *decision-making algorithm* (DMA) was developed by *Parfiniewicz* (1976). Three components were applied in his method: the horizontal check of height and temperature, and the hydrostatical check.

All the existing versions of CQC consist of at least these three components. The most advanced CQC contains two additional components: vertical check of height and temperature.

Many specialists still consider the quality control as a secondary task. This is the reason why CQC algorithms of other radiosonde data (wind, humidity) have not been developed yet. Therefore, CQC of height and temperature data remained the only operationally functioning CQC (see further details in *Gandin*, 1988).

Instead of developing the existing system, the design of a new quality control system was started at NMC, Washington, D. C. in 1988. NMC decided to design and implement a comprehensive hydrostatic quality control (CHQC) which uses only hydrostatic check, but it still contains an advanced DMA. This DMA is capable of detecting and correcting the gross hydrostatic errors. This is the first step to design a complex multicomponent quality control, which still has to include horizontal and vertical check of height and temperature without the hydrostatic check. The CHQC was put into operation at the end of 1988. The experiments showed that the data corrected by CHQC were never rejected by subsequent checks.

There exists a kind of man-machine interaction in the process of CHQC. It appears in all cases when CHQC cannot correct the data alone, and specialists make the final decisions. Using this procedure, there is a possibility to correct more erroneous data. There is no doubt that in the future, when the hydrostatic check is used together with statistical interpolation checking, still more wrong data can be corrected automatically.

In Hungary, *Ozorai* (1972) and *Dévényi* (1983) have made attempts at automatic hydrostatic quality control so far. Though our method in its present form, which is described in the next section, is based on hydrostatic control only, a complex quality control method must contain both horizontal and vertical check. Data check in the horizontal direction can be realized, e.g., by using Bayesian quality control methods (*Lorenc* and *Hammon*, 1988). The Bayesian method assumes that observation errors can be described by a probability distribution, which is a combination of a Gaussian white noise and the uniform distribution, the latter representing gross errors.

2. *The method*

Let us apply the hydrostatic equation to a layer between two adjacent mandatory surfaces, and let us compose the difference between the two sides of the equation. Furthermore, let us define this difference as a hydrostatic residual. The CHQC is based on the examination of these residuals.

Integrating the hydrostatic equation through a layer between the isobaric surfaces (p_i, p_{i+1}), and applying the following formulas

$$A_{i,\,i+1} = (RT_0/g)\ln(p_i/p_{i+1}), \tag{1}$$

$$B_{i,\,i+1} = (R/2g)\ln(p_i/p_{i+1}), \tag{2}$$

where T_0=213.15 K, g is the acceleration of gravity, R is the gas constant for dry air, and p_i, p_{i+1} are pressure of the ith and $i+1$th surfaces, then the hydrostatic equation can be written in the following form

$$z_{i+1} - z_i = A_{i,i+1} + B_{i,i+1}[(T_i + T_{i+1}) + 2t_{i,i+1}], \tag{3}$$

where z is height (dkm) and T is temperature (°C).

The term $t_{i,i+1}$ consists of three factors: neglect of humidity and roundoff errors, and the use of mandatory levels only (this results from allowing the nonlinearity of temperature with the logarithm of pressure).

The hydrostatic residual in terms of height and temperature is defined as

$$S_{i,i+1} = z_{i,i+1} - z_i - A_{i,i+1} - B_{i,i+1}(T_i + T_{i+1}) \tag{4}$$

and

$$X_{i,i+1} = (z_{i+1} - z_i)D_{i,i+1} - (T_i + T_{i+1}) - 2T_0, \tag{5}$$

where $D_{i,i+1} = 1/B_{i,i+1}$ ($X_{i,i+1}$ stems from dividing $S_{i,i+1}$ by $B_{i,i+1}$).

If height and temperature data contain gross errors,

$$z_i = \hat{z}_i + z_i' \qquad T_i = \hat{T}_i + T_i', \tag{6}$$

$$Z_{i+1} = \hat{Z}_{i+1} + Z_{i+1}' \qquad T_{i+1} = \hat{T}_{i+1} + T_{i+1}', \tag{7}$$

where $\hat{z}_i$, $\hat{z}_{i+1}$, $\hat{T}_i$, $\hat{T}_{i+1}$ are values, which exactly satisfy the hydrostatic balance (primed values are gross errors), then residuals in terms of gross errors are

$$S_{i,i+1} = z_{i+1}' - z_i' - B_{i,i+1}(T_i' + T_{i+1}' - 2t_{i,i+1}), \tag{8}$$

$$X_{i,i+1} = (z_{i+1}' - z_i')D_{i,i+1} - (T_i' + T_{i+1}' - 2t_{i,i+1}). \tag{9}$$

To detect the errors and error types, a "backward" problem has to be solved, because it is an easier task to approximately determine what the residuals should be for a particular error or several errors. The actual problem is to find the errors which are obtained by a particular pattern of residuals.

The DMA of CHQC examines four levels (three layers) at the same time (*Fig. 2.*). This "template" progressively moves upward along the profile, while looking for errors on the basis of a definite pattern of residuals. After reaching the top of the profile, a second pass is made through the data in order to examine them more precisely. To find an error which has to be corrected, existence and magnitude conditions have to be satisfied. The DMA can separate errors of different types by existence conditions, while magnitude conditions assure that any suspected error has a sufficient size (not the result of the $t_{i,i+1}$s).

Formulas for provisional correction (*Table 1*) in terms of temperature have been derived by minimizing the sum of the squares of the resulting residuals.

We have checked the accuracy of the equation with disturbing some data and deducing the equations. We can get the formulas for existence conditions (*Table 2*): by writing Eqs. (8) or (9) for the layer which contained an erroneous level,

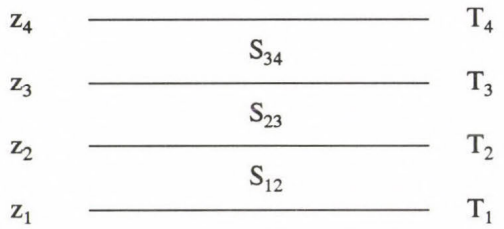

Fig. 2. The template.

eliminating the errors (e.g. by Gaussian elimination), then squaring the obtained equations and averaging over many realizations. We have deduced these formulas, too. The magnitude conditions can be seen in *Table 3*.

Table 1. Formulas for provisional corrections

Type	Formulas for provisional corrections
1	$z_3' = (D_{34}X_{34} - D_{23}X_{23})/(D_{34}^2 + D_{23}^2)$
2	$T_3' = (X_{23} + X_{34})/2$
3	$z_3' = (B_{23}S_{34} - B_{34}S_{23})/(B_{23} + B_{34})$ $T_3' = (S_{23} + S_{34})/(B_{23} + B_{34})$
7	$z_2' = (-D_{12}(D_{23}^2 + D_{34}^2)X_{12} + D_{23}D_{34}^2X_{23} + D_{23}^2D_{34}X_{34})/$ $((D_{12}^2 + D_{34}^2)D_{23}^2 + D_{12}^2D_{34}^2)$ $z_3' = (-D_{12}D_{23}^2X_{12} - D_{23}D_{12}^2X_{23} + (D_{12}^2 + D_{23}^2)D_{34}X_{34})/$ $((D_{12}^2 + D_{34}^2)D_{23}^2 + D_{12}^2D_{34}^2)$
8	$T_2' = (2X_{12} + X_{23} - X_{34})/3$ $T_3' = (2X_{34} + X_{23} - X_{12})/3$
9	$z_2' = (D_{23}X_{23} - 2D_{12}X_{12} - D_{23}X_{34})/(2D_{12}^2 + D_{23}^2)$ $T_3' = (D_{12}^2X_{23} + D_{12}D_{23}X_{12} + (D_{12}^2 + D_{23}^2)X_{34})/(2D_{12}^2 + D_{23}^2)$
10	$T_2' = ((D_{23}^2 + D_{34}^2)X_{12} + D_{34}^2X_{23} + D_{23}D_{34}X_{34})/(D_{23}^2 + 2D_{34}^2)$ $z_3' = (D_{23}X_{12} + 2D_{34}X_{34} - D_{23}X_{23})/(D_{23}^2 + 2D_{34}^2)$

We can get a huge residual if one of the four values in question for the hydrostatic residual (two heights and two temperatures) is distorted by a gross

communication-related error. Accordingly, if the erroneous level is not the highest or the lowest reported one, then a large hydrostatic residual for the two adjacent layers contained this level will be involved by an error in either height

Table 2. Existence conditions

Type	Existence conditions
1	$\lvert S_{23} + S_{34} \rvert < 2\bar{t}_{all}(B_{23}^2 + B_{34}^2)^{1/2}$
2	$\lvert X_{23} + X_{34} \rvert < 2\bar{t}_{all}$
7	$\lvert S_{12} + S_{23} + S_{34} \rvert < 2\bar{t}_{all}(B_{12}^2 + B_{23}^2 + B_{34}^2)^{1/2}$
8	$\lvert X_{12} - X_{23} + X_{34} \rvert < 2\bar{t}_{all}3^{1/2}$
9	$\lvert S_{12} + S_{23} - (B_{23}/B_{34})S_{34} \rvert < 2\bar{t}_{all}(B_{12}^2 + 2B_{23}^2)^{1/2}$
10	$\lvert S_{23} + S_{34} - (B_{23}/B_{12})S_{12} \rvert < 2\bar{t}_{all}(B_{34}^2 + 2B_{23}^2)^{1/2}$

or temperature at this level. Examining these residuals, DMA has to decide whether height or temperature or both are wrong in the level.

Table 3. Magnitude conditions

Type	Magnitude conditions
1	$\lvert z_3' \rvert > 2\bar{t}_{all}(B_{23}^2 + B_{34}^2)^{1/2}$
2	$\lvert T_3' \rvert > 2\bar{t}_{all}$
7	$\lvert S_{12} \rvert > S_{12}^{thres}$ and $\lvert S_{34} \rvert > S_{34}^{thres}$
8	$\lvert X_{12} \rvert > 2\bar{t}_{all}$ and $\lvert X_{34} \rvert > 2\bar{t}_{all}$
9	$\lvert S_{12} \rvert > S_{12}^{thres}$ and $\lvert X_{34} \rvert > 2\bar{t}_{all}$
10	$\lvert X_{12} \rvert > 2\bar{t}_{all}$ and $\lvert S_{34} \rvert > S_{34}^{thres}$

If so, *Type 1* is an error at a single, isolated height, resulting in huge hydrostatic residuals of opposite sign in the adjacent layers.

In the same way, let us define *Type 2*, as an error in a single, isolated

temperature, but this type of error results in large hydrostatic residuals of the same sign in the adjacent layers. If both height and temperature are wrong, then we can consider it as a *Type 3* error.

The CHQC developed by *Gandin* and *Collins* (1990) analyses four levels (template) at the same time, and DMA defines the error types in the third level of the template. However, it is not possible to detect isolated errors of the second level of the profile. In order to avoid this problem, *Gandin* and *Collins* introduced an additional test of the profile by scanning it downwards, starting from the top level. Instead of this, we have introduced additional error types to examine the second level of the template by the same method as analysing the third one. Consequently, *Types 11, 12* and *13* were introduced similarly to *Types 1, 2* and *3*. We have decided to follow this way, because it is simpler than Gandin's and Collins' method, and introducing the new types was more advantageous for our purposes.

A gross error in either height or temperature at the lowest level leads to a large hydrostatic residual. This is the *Type 4* error. The CHQC DMA is unable to decide which of the two values is wrong (maybe both of them). Unique decision for this is a much more complex procedure of correction, which must be combined with other checking residuals. Since it has not been implemented, our DMA rejects the lowest level in this case.

The analogy of *Type 4* error is a single large residual for the highest layer, when either temperature or height of the highest level (or both of them) is wrong (*Type 5* error).

A gross error in the computation (or documenting) of the layer's thickness may result in a large hydrostatic residual for only one layer. Let us define this as *Type 6* error. If this kind of error occurs, the height of all surfaces above this layer should be corrected. To make any correction automatically based on only one residual, is risky, so this case was not investigated. We can neglect it because the statistical calculation demonstrates (*Gandin*, 1991) that *Type 6* of errors happens relatively seldom. One can say that the computational errors represent a small part of hydrostatic errors. In the future, if a hydrostatic QC is completed with other checking systems, for example in case of Type 6 errors with height increments and horizontal statistical interpolation residuals at several levels (*Collins*, 1991), more corrections can be checked.

Experiment shows that most of the hydrostatic errors are telecommunication related. A part of these belongs to the category called "simple" errors. It appears during processing the data at the station or in the course of communicating them. Simple error is (1) an error of a single digit, (2) interchange of digits and (3) sign error of temperature or any combinations of these.

Both height and temperature at a level have to exist in the report to be controlled hydrostatically. If any of them (or both of them) is missing and both neighbours below and above are not empty, that level is called a missing level. One or several of missing levels in a report does not prevent the DMA from

performing the QC of existing levels. However, it may happen that a report contains the same parameter of several missing levels, then the report contains a "data-hole". We do not examine this case. Nevertheless, a lack of temperature or height of one level is defined as a *Type 14* error.

Two or more hydrostatic errors seldom occur in a report, and if at least one error-free level exists between those containing errors, then DMA can detect it successively and, if possible, DMA can correct them. It is different from the case when two adjacent mandatory levels contain gross errors. In this case DMA has to analyze three adjacent layers (4 levels) simultaneously, instead of two adjacent layers (for this reason the template consists of 4 levels). If gross errors were found independently of each other, these cases occur much more often than they would. The NMC's CHQC (and also our method) is able to deal with the next four types: two adjacent height errors (*Type 7*), two adjacent temperature errors (*Type 8*), adjacent errors in height below and temperature above (*Type 9*), and *vice versa* (*Type 10*). Every type of errors is summarized in *Table 4*.

What happens if there are three or more hydrostatic errors at adjacent levels? These situations are more complicated cases, so CHQC is unable to treat them because too many branches of the DMA would have to be added in order

Table 4. Error types

Type	Description
1	Large isolated height error
2	Large isolated temperature error
3	Error in height and temperature of the same level
4	Error in height or temperature or both of the highest level
5	Error in height or temperature or both of the lowest level
6	Computational error in a layer thickness (not detected)
7	Errors in heights of two adjacent levels
8	Errors in temperatures of two adjacent levels
9	Adjacent errors in height below and temperature above
10	Adjacent errors in temperature below and height above
11	Type 1 error in the second reported level
12	Type 2 error in the second reported level
13	Type 13 error in the second reported level
14	Lack of temperature or height in one level

to achieve this aim, and still there would remain more complicated combinations of errors not treatable by the DMA. Such combinations happen very seldom. In the present stage of DMA, in these most complicated cases human help is necessary .

3. *The decision-making algorithm*

The reason of describing the DMA in more detail is that a very specialized logic is necessary for hydrostatic error correction. In spite of the fact that DMA is relatively complicated, the required computer time is minimal since only suspected reports are examined.

First of all, error determination begins with computing residuals for each profile of heights and temperatures, and looking for large residuals. If DMA finds a large residual in a profile, it is examined further. The selection of suspicious, erroneous profiles is done by using empirical thresholds. These thresholds are derived from a residual of about seven times the standard deviation of error-free data published by *Gandin* and *Collins* (1990). We need the threshold values when the profile contains isolated missing levels. In this case, we had to derive these values from thresholds of available two adjacent layers. Thus, we had to determine a residual of about seven times the standard deviation of the values in the absence of gross errors for sum of these adjacent layers. If these residuals can be considered as independent random variables then a threshold value for a sum of two adjacent layers is the sum of the two threshold values. On the other hand, these residuals are not independent in general, so the required values have to be smaller than the sum of the two threshold values. Our experiments have shown that the mean of the maximum and sum of these two threshold values is an appropriate choice as a threshold value of the missing layer. These values for each mandatory layer (and also for isolated missing layers) can be found in *Table 5*.

Table 5. Threshold residuals (also for layers containing one missing level)

Pressure layers hPa	Threshold residuals m	Pressure layers hPa	Threshold residuals m
1000–925	40	1000–850	65
925–850	30	925–700	50
850–700	35	850–500	70
700–500	50	700–400	70
500–400	35	500–300	60
400–300	40	400–250	60
300–250	35	300–200	60
250–200	40	250–150	70
200–150	50	200–100	110
150–100	85		

Errors of *Types 1, 2* and *7* to *10* must satisfy existence and magnitude conditions. It also occurs that both height and temperature are erroneous at the same level. Investigations (*Gandin* and *Collins*, 1990) show that two adjacent residuals containing this level are large, but the existence conditions are not satisfied for a height or temperature correction (*Type 3* error). In this case there is a pair of height and temperature that will make the residuals zero. This pair is suggested as height and temperature corrections (Table 1).

We have already mentioned that a radiosonde profile is examined by progressively moving the template upward from the lowest existing level. First, our DMA computes hydrostatic residuals with omitting missing levels (if any). If a large residual is found in a report, it begins to examine errors (*Types 4, 5* and *14* errors) which cannot be corrected. In this case the DMA rejects the erroneous level. In the case of *Type 3* error (and *Type 13* error) the operator decides to accept or to reject the suggested correction. After the detection of the errors that cannot be corrected, correctable ones are searched on the bases of existence and magnitude conditions.

It also happens that more than one error type satisfies both conditions. In this case the DMA calculates the ratio of two sides of the existence condition for every satisfied type and then accepts the correction which has given the largest value of ratio (fulfils existence condition most strongly).

Sometimes Arctic stations report 700 hPa heights less than 2400 m in winter, but the thousand's digit of the 700 hPa height is not included in the coded message. Therefore, in general, 3 is added during the decoding process. Then the DMA can correct safely these heights by 1000 m.

Finally, our algorithm accepts the proposed corrections only if the temperature correction is at least 10°*C* in magnitude, and height correction is at least 30 m at 1000–700 hPa, and at least 90 m at the other levels. Multiple corrections (*7–10 types*) are not made if both are small, as defined above.

In some rare cases, residuals of *7* and *8 types* or *9* and *10 types* are the same. This case occurs when the median of the three residuals is small. Then DMA is unable to distinguish between these two types.

4. Examples for the different error types

In this section we show the possibilities and limitation of the method. The examples are partly derived from real cases. On the other hand, we have also artificially introduced errors for some error types. Information in the examples includes the date and time; station identification number, pressure p (hPa); height z (m); temperature T (°C); residual S (decameter); height correction *ZCOR* (m) (if any); temperature correction *TCOR* (°C) (if any); and error type. First examples show the most frequent errors, while rarely occurring errors are introduced by ourselves.

Accordingly, variable forms of *Type 1* (or *Type 11*) can be seen in examples 1–4 and then 2 error types follow.

Example 1: *Type 1* error; single digit error. Operator makes "simple" correction (it is clear from roundoff correction); height at 500 hPa is corrected with 2000 m.

10.11.1992		00 UTC		Barencburg (20 107)		
p	z	T	S	ZCOR	TCOR	Type
850	1250	-9.4				0
			0.12			
700	2740	-13.4				0
			-199.85			
500	3230	-28.0		2000		1
			200.53			
400	6800	-39.6				0
			-0.02			

Example 2: *Type 1* error; general error type. This correction can be executed.

10.11.1992		00 UTC		Rjazan' (27 731)		
p	z	T	S	ZCOR	TCOR	Type
400	6940	-40.6				0
			-1.11			
300	9840	-52.2				0
			18.25			
250	10200	-53.2		-180		1
			-17.92			
200	11460	-52.8				0
			0.79			

Example 3: *Type 1* error; small height correction. The height correction is 40 m at 400 hPa, so it is smaller than 90 m (limited correction). No correction is made by our program in this case.

29.09.1992		00 UTC		Barencburg (20 107)		
p	z	T	S	ZCOR	TCOR	Type
700	2940	-12.4				0
			-0.33			
500	5440	-26.0				0
			4.44			
400	7070	-35.2		-40		0
			-3.41			
300	8990	-47.4				0
			-			

Example 4: *Type 11* error; the second level of report contains height error (this type was introduced by us). Operator corrects the height at 700 hPa with -100 m.

29.09.1992	00 UTC		Simferopol' (33 946)			
p	z	T	S	ZCOR	TCOR	Type
1000	–	–				0
925	–	–				0
850	1514	11.3				0
			10.31			
700	3206	1.1		-100		11
			-7.9			
500	5750	-15.2				0
			0.23			

Example 5: *Type 2* error; sign correction. -52°C correction is proposed at 400 hPa instead of 25.9°C. Obviously this is a "simple" error.

30.09.1992	12 UTC		Constanta (15 480)			
p	z	T	S	ZCOR	TCOR	Type
700	3159	1.3				0
			-0.01			0
500	5780	-15.8				0
			-16.87			
400	7430	25.9			-52	2
			-22.43			
300	9440	-42.4				0
			0.42			

As already mentioned, DMA can correct the 7–10 error types, too. The next two examples show *Types 7* and *8* errors of them.

Example 6: *Type 7* error; height of two adjacent levels are erroneous.

29.09.1992	00 UTC		Bucuresti (15 420)			
p	z	T	S	ZCOR	TCOR	Type
			-0.38			
700	3130	0.7				0
			-399.5			
500	1760	-14.4		4000		7
			200.29			
400	5410	-28.0		2000		7
			200.13			
300	9410	-44.0				0
			0.06			

Example 7: We have added 20°C at 300 hPa and -30°C at 400 hPa to the temperature. Then the template contained two error types: *Type 1* and *Type 8*, but our program suggested *Type 8*, because this type satisfies rather the existence condition.

29.10.1992	12 UTC			Bjornoya (01 028)		
p	z	T	S	ZCOR	TCOR	Type
			-0.34			
500	5140	-40.2				0
			-9.65			
400	6300	-79.8			30	8
			-4.42			
300	9480	-38.0		-50	-20	1, 8
			-5.69			
250	9630	-56.4				0
			0.86			

Hereafter we show examples for the correction, which cannot be made by DMA. Example 8: *Type 7* and *Type 8* errors. In this example both types satisfy both conditions, because hydrostatic control is unable to distinguish whether height errors of two adjacent levels have the same value and same sign, or temperature errors of two adjacent levels have the same value but opposite sign. In this case the medium residual will be small, while the other two residuals will have the same values and sign. Then our method does not correct them. (The situation is similar for the *Type 9* and *Type 10* errors.)

27.10.1992	12 UTC			Isparta (17 240)		
p	z	T	S	ZCOR	TCOR	Type
			-0.38			
400	7330	-27.8				0
			-7.97			
300	9260	-41.6		80	-19	7, 8
			-0.67			
250	10480	-50.4		70	21	7, 8
			6.84			
200	11970	-61.0				0
			2.36			

Example 9: *Type 5* error. The highest level is wrong. Operator deleted this level from the report. Similar to *Type 4* error.

30.09.1992	12 UTC			Simferopol' (33 946)		
p	z	T	S	ZCOR	TCOR	Type
850	1367	-4.0				0
			-2.64			
700	2871	-4.2				0
			-5.91			
500	5330	-31.2				5
400	-	-				

Example 10: We damaged the temperature by 20°C at 850 hPa and the height by 1000 m at 500 hPa. The proposed corrections can be seen in the example. Operator will correct the temperature at 850 hPa and the height at 500 hPa, because *Type 1* satisfies rather the existence condition. Therefore correction of *Type 7* error at 700 hPa is not performed.

17.11.1992	00 UTC			Vienna (11 035)		
p	z	T	S	ZCOR	TCOR	Type
925	636	4.3				0
			-2.36			
850	1320	20.7			-18	12
			-5.06			
700	2868	-7.0		44		7
			101.15			
500	6430	-20.6		-1000		1, 7
			-99.24			
400	7050	-32.4				0
			0.34			

Example 11: *Type 3* error; height was changed by 1000 m and the temperature by 20°C at 500 hPa. This type of error seldom occurs and the proposed corrections are not reliable, so operator has to decide to correct them or not. In the example the corrections are good.

17.11.1992	00 UTC			Bjornoya (01 028)		
p	z	T	S	ZCOR	TCOR	Type
850	1386	-5.6				0
			0.51			
700	2897	-11.2				0
			92.77			
500	6430	-20.6		-1000	-14	3
			-104.2			
400	6980	-37.4				0
			0.21			

Example 12: *Type 6* error (computation error of layer thickness). Every height at 500–250 hPa was damaged by 100 m. Our method does not make correction, as explained above. A typical large residual can be seen in the example.

30.09.1992	12 UTC			Simferopol' (33 946)		
p	z	T	S	ZCOR	TCOR	Type
1000	-	-				
925	-	-				
850	1321	2.5				
			0.01			
700	2858	-8.4				
			9.81			
500	5490	-23.8				
			0.45			
400	7090	-34.4				
			-0.31			
300	9030	-50.8				
			-0.33			
250	10200	-56.2				
			-11.55			
200	11510	-54.0				
			0.7			

5. Results and conclusions

The information on the CHQC at NMC was produced automatically from the monthly summaries by CHQC Performance Statistics Code between May 1989 and April 1991 (*Gandin*, 1991). These summaries contain not only information about all suspected and corrected data, but also some statistics about errors of different types. These statistics were made over different regions of the globe, and at different elevations. The main purpose of the monthly summaries is to create error statistics in operationally received radiosonde reports on mandatory level heights and temperatures, and of the CHQC performance in correcting these errors. On the basis of some globally averaged CHQC statistics, about 7% of radiosonde reports are suspected by the CHQC and about half of these can be corrected by CHQC alone. In details: ratio of reports with *Type 1* errors is about 26.9%, with *Type 2* errors is about 23.1%, and with errors at two adjacent mandatory levels (*Types 7–10*) is about 4%.

These statistics are made over the globe, so there is a strong geographical inhomogeneity in the occurrence of hydrostatic errors. The reason of this inhomogeneity is the overwhelming majority of "hydrostatic" errors originating from countries where communication processes are not, or incompletely, computerized. In these regions of the globe, the rate of gross hydrostatic errors is higher than in the regions where the processing of radiosonde measurement is entirely automatized.

We are particularly interested in the statistics for Eastern European and Western European regions because our operational NWP model makes forecasts over these regions. Reports from European regions contain 4.7% of hydrostatic error (*Gandin*, 1991). We have obtained smaller values by running our operational model, but we have to take into account that the hydrostatic control is preceeded by a "formal" control, which checks decoding errors.

We are also interested in the information about errors in operationally received radiosonde reports for our model. So we made statistics for the period between June 1992 and May 1993. Two aspects were examined: (1) missing of radiosonde reports of every single station and every part (A, B, C, D) of the reports, and (2) erroneous radiosonde reports of every single station by error types and mandatory levels. We have divided the area used by our model into three regions: Western Europe (I), Central Europe (II) and Eastern Europe (III) (*Fig. 3*). We received most of the reports from region I and these reports contained the least errors in contrast with region III (*Table 6*). Average over the whole area showed that 102 reports were complete (received and included part (*a*) from the available 124 reports, and 3 of them were erroneous. It can be seen in *Table 6b* that the number of presence of *Types 1* and *2* errors and other types altogether is nearly the same, and missing level occurred in a significant

number. The main reason of this is the lack of 925 hPa level (as it can also be seen from the error statistics in *Table 6c* and *Table 7*). The results of the latter

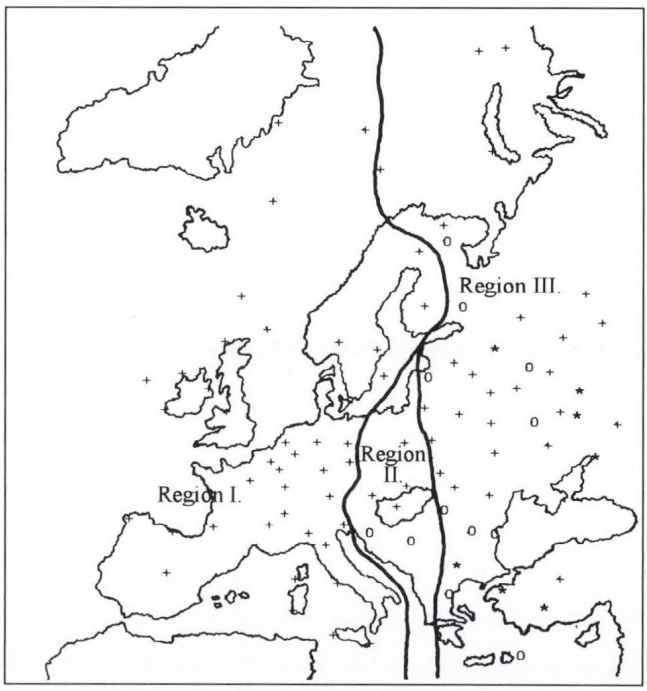

Fig. 3. Summary of statistics for stations in Europe: o stations, not disseminated reports in most cases; * stations, disseminated erroneous data in most cases.

Table 6. Some avareged CHQC statistics (every value is given in percent)

	Region I (61)	Region II (9)	Region III (60)	Whole area
(a)				
Available reports	90	80	73	82
Missing reports	8	19	23	15
Missing part A	2	1	4	3
Error contained reports	1.4	1.3	3.4	2.2
(b)				
Distribution of errors by types	Region I	Region II	Region III	Whole area
Type 1 and 2	34	25	41	38
(Type 1, Type 2)	(28, 5)	(16, 8)	(28, 13)	(27, 8)
Other types	24	30	31	33
Missing level	42	45	28	27

Continued Table 6

(c)

Distribution of errors by level (hPa)	Region I	Region II	Region III	Whole area
1000	0	0	0	0
925	28	39	44	39
850	2	2	5	4
700	14	2	7	9
500	10	13	11	10
400	8	12	7	8
300	11	10	9	9
250	8	8	6	7
200	9	8	4	6
150	8	4	4	5
100	2	2	3	3

two tables justify a systematic 1000 m decoding error of 700 hPa level, so *Type 1* error often occurred in this level (mainly in winter). This table shows that 500 hPa level often was the highest reported level and it was at the same time frequently erroneous.

Our plans for the future are supplementing the procedure with a horizontal check and further development of this method.

Table 7. Distribution of errors by types and levels (every value is given in percent).

Level (hPA)	Type 1	2	3	4	5	6	7	8	9	10	14
1000	0	0	0	0.3	0	0	0	0	0	0	0
925	3.9	0	0	3.6	0	0	0	0	0	0	21.7
850	1.3	0.8	0.1	1.8	0	0	0.1	0	0	0.1	0.2
700	9.0	1.2	0	0.1	0	0	0.3	0.1	0.2	0.1	0.5
500	2.6	1.9	0	0	7.6	0	0.3	0.1	0.3	0.2	0.4
400	2.3	1.9	0	0	0.5	0	0.5	0.6	0.3	0.3	1.9
300	2.6	2.0	0	0	0.3	0	0.8	1.2	0.2	0.1	2.3
250	2.1	1.3	0.1	0	0.2	0	0.5	0.9	0.1	0	2.1
200	2.2	1.0	0	0	0.5	0	0.3	0.3	0.1	0	1.9
150	1.7	0.8	0	0	0.4	0	0.2	0.1	0.1	0	1.9
100	0	0	0	0	4.0	0	0	0	0	0	0

Acknowledgements—I would like to thank, first of all, to *István Ihász* and *Gábor Radnóti* for their help during my work. Also, I would like to thank to *Dr. Dezső Dévényi* for his suggestions and *Prof. György Major* for his support.

References

Belousov, S.L., Gandin, L.S. and *Mashkovich, S.A.*, 1968: *Computer Processing of Current Meteorological Data* (in Russian). Gidrometeoizdat (Meteor. Trans. No. 18, 1972. Canada Dept. of the Enviroment, Atmospheric Enviroment Service, Downsview, Ontario).

Bergthorson, P. and *Döös, B.R.*, 1955: Numerical weather map analysis. *Tellus 7*, 367-374.

Collins, W.G., 1991: Complex quality control of rawinsonde heights and temperatures at the National Meteorological Center. *Preprints, 9th Conference on Numerical Weather Prediction*, Denver, Colorado, 14-18 October, 15-18.

Dévényi, D., 1983: Methods of automatic control of operative meteorological information (in Hungarian). *Meteorológiai Tanulmányok* No. 45, OMSZ, Budapest.

ECMWF, 1985: *Workshop on the Use and Quality Control of Meteorological Observation.* Readings, U. K., European Centre for Medium Range Weather Forecast.

Gandin, L.S., 1988: Complex quality control of meteorological observations. *Mon. Wea. Rev. 116*, 1138-1156.

Gandin, L.S. and *Collins, W. G.*, 1990: Comprehensive hydrostatic quality control at the National Meteorological Center. *Mon. Wea. Rev. 118*, 2752-2767.

Gandin, L.S., 1991: Two years of operational comprehensive quality control at the National Meteorological Center. *Preprints, 9th Conference on Numerical Weather Prediction*, Denver, Colorado, 14-18 October, 11-14.

Gilchrist, B. and *Cressman, G.P.*, 1954: An experiment in objective analyses. *Tellus 6*, 309-318.

Lorenc, A.C., Rutherford, I. and *Larsen, G.*, 1977: The ECMWF analysis and data assimilation scheme—Analysis of mass and wind fields. European Centre for Medium Range Weather Forecasts, Reading, Berkshire, U.K., *Tech. Rep.* No. 6.

Lorenc, A.C. and *Hammon, O.*, 1988: Objective quality control of observations using Bayesian methods. Theory, and a practical implementation. *Quart. J. Roy. Meteorol. Soc. 114*, 515-543.

Ozorai, Z., 1972: Control of the calculation of the attitudes included in TEMP messages (in Hungarian). *Időjárás 76*, 326-333.

Parfiniewicz, J., 1976: *Complex Quality Control of Upper Air Information* (in Russian). Methodical guidelines. Hidrometeorological Center. Gidrometeoizdat, Leningrad.

IDŐJÁRÁS

Quarterly Journal of the Hungarian Meteorological Service
Vol. 97, No. 4, October–December 1993

Application of satellite digital images in the investigation of the daily temperature amplitude of the surface

I. Csiszár, E. Fejes, J. Kerényi and **A. Rimóczi-Paál**

Satellite Research Laboratory, Hungarian Meteorological Service,
P.O. Box 32, H-1675 Budapest, Hungary

(Manuscript received 14 January 1993; in final form 10 November 1993)

Abstract—Digital data of the meteorological satellites give new opportunities to investigate the heat and radiation budget of the Earth-atmosphere system. The good spatial resolution of AVHRR (*Advanced Very High Resolution Radiometer*) on board the polar orbiting NOAA satellites makes it possible to construct detailed temperature, vegetation and radiation maps of Hungary and to search for statistical connections between them. A new project sponsored by the *Hungarian Scientific Found* started to determine the relationship between the daily changes of surface temperature and other meteorological parameters. In this paper the methods of the calculation of temperature, vegetation index and radiation balance components and the first results are presented.

Key-words: daily temperature amplitude, NOAA and METEOSAT digital images, radiation balance, vegetation index.

1. Introduction

The exact knowledge of the heat budget of the surface is very important in both climatology and agriculture. Variation of the temperature of the surface in different areas of Hungary on cloudless days can give important information about the heat capacity and characteristics of different soil types or vegetation. Last year a four-year investigation sponsored by the Hungarian Scientific Found (Project OTKA No. 2024) started to determine the relationship between temperature variation and other meteorological parameters. Digital images of the meteorological satellites give a new opportunity to construct maps of the temperature distribution and variability for the whole country. In this investigation Hungary and its surroundings are covered by squares of 20 by 20 kilometers and each area can be studied separately using digital METEOSAT and NOAA/AVHRR images. Without applying satellite images a large series of local measurements would be necessary to obtain good spatial resolution. All

the satellite images were acquired at the digital receiving station of the Hungarian Meteorological Service.

In this paper the method, the data basis and the first results are presented.

2. *Determination of the data basis*

2.1 Vegetation index

The NOAA/AVHRR measurements are suitable to give objective information about the development and the geographical distribution of the vegetation due to their good spatial resolution. From the five channels the visible (VIS) and the near infrared (NIR) bands give the opportunity to calculate the vegetation index. The first spectral channel is in that part of the spectrum where chlorophyll causes considerable absorption of incoming radiation, whereas the second one is in a spectral region where spongy mesophyll leaf structure leads to significant reflectance (*Justice et al.*, 1985). This contrast between the two channel responses can be conveniently shown by a ratio transform, i.e. dividing one channel by the other. Several ratio transforms have been proposed for the study of different land surfaces (*Tucker*, 1979). The normalized difference vegetation index (*NDVI*) is one of such ratios, which has been shown to be highly correlated with vegetation parameters such as biomass and green-leaf area and hence it is of considerable value for the investigation of the vegetation (*Jackson et al.* 1983)

$$NDVI = (X_{NIR} - X_{VIS})/(X_{NIR} + X_{VIS}), \tag{1}$$

here *NDVI* is the normalized differential vegetation index, X_{NIR} is the brightness value (count) in the near-infrared spectral band, X_{VIS} is the brightness value (count) in the visible spectral band.

The value of the vegetation index is between -1 and $+1$. Clouds, water and snow have larger reflectances in the visible than in the near infrared, so for these features *NDVI* is negative. Rock and bare soil have similar reflectances in these two bands and the vegetation index is near zero (*Yates et al.*, 1984). In scenes with vegetation, *NDVI* ranges from 0.1 to 0.6; the higher values are associated with greater density and greenness of the plant canopy. The vegetation index has large values when the vegetation is well developed. The largest values indicate forests and the 0 values are water surfaces or clouds.

2.2 Radiation balance components

The radiation balance at the surface is calculated from the global radiation,

reflected solar radiation, longwave radiation reaching the surface and emission of the surface

$$R = G(1 - RS) + (LD - LU), \tag{2}$$

where R is the radiation balance of the surface, G is the global radiation, RS is the surface albedo, LD is the longwave radiation reaching the surface, LU is the longwave radiation emitted by the surface.

The solar radiation reaching the surface is calculated by the empirical multilinear equation (*Rimóczi-Paál,* 1989)

$$G = 49.5 - 4.65B + 32.5 \cos h. \tag{3}$$

Here G is the global radiation given in percents of the solar radiation at the top of the atmosphere, B is the relative brightness characterizing the cloud coverage and transmittance and h is the solar zenith angle.

The definition of the relative brightness is (*Rimóczi-Paál,* 1985)

$$B = (F - F_{\min})/(F_{\max} - F_{\min})10, \tag{4}$$

where F is the outgoing flux over the investigated area, $F_{\min}$ is the outgoing flux over a cloudless area (near the investigated area), $F_{\max}$ is the outgoing flux over a totally cloudy area (near the investigated area).

The empirical constants in Eq. (3) were determined from a data set of two years from surface measurements and from redigitized analogue data of METEOSAT 2 satellite. Using Eq. (4) the relative brightness values are calculated from digital visible images of METEOSAT 4 satellite.

The surface albedo is determined from the minimum brightness values of an extended area in the southern part of Central Europe. The brightness of the cloudfree surface is chosen by using histograms in the range of 16–48 counts. In most cases the first peak is the sea surface and the second one is the brightness of the land surface.

The surface albedo (RS) is approximated by Eq. (5)

$$RS = 1.25\, CC + 0.07, \tag{5}$$

$$CC = (B_{\min} - C_0)/(I_0 \cos h \sin Z\, RF), \tag{6}$$

where $B_{\min}$ is the minimum surface brightness, C_0 is the count of the space, I_0 is the solar constant, h is the solar zenith angle, RF is the normalized Sun-Earth distance, Z is the satellite zenith angle.

The constants are determined from case-studies by comparing the estimated values to the measurements.

The longwave radiation reaching the surface is calculated by a radiative transfer model adapted from the University of St. Petersburg (*Práger* and *Kovács*, 1988), which applies broad band approximation with 17 spectral intervals. The humidity and temperature profiles are taken from radiosonde observations of Budapest. The effects of CO_2, O_3, CH_4, NO_2, Freon11, Freon12 and the aerosols are taken into account. The profiles of the trace gases are considered as climatological averages. The effect of the clouds is approximated by a simple cloud parameterization. The cloud parameter *BC* is calculated by Eq. (7)

$$BC = 0.05\, B\,(B_{\min}/B_{\max}) + RS, \tag{7}$$

where $B_{\min}$ is the minimum brightness, $B_{\max}$ is the maximum brightness, B is the relative brightness like in Eq. (4), *RS* is the surface albedo.

The cloud amounts and the cloud levels are taken from *Table 1*. For example if the *BC* is 0.35, then a cloud amount of *B/2* is considered in the middle level. This simple cloud parameterization based only on cloud albedo is subjective. Our purpose is to construct an objective cloud-parameterization using both albedo and cloud temperature.

Table 1. Cloud amount and level from the BC cloud parameter

BC	>0.50	0.40–0.50	0.30–0.40	0.24–0.30	<0.24
Low	B/2	B/3	–	–	–
Middle	B/2	B/3	B/2	–	–
High	–	B/3	–	B/2	–

The values of the longwave radiation reaching the surface estimated by the radiative transfer model in the grid point containing Budapest were significantly lower than the measured values. Thus a magnification factor of 1.2 had to be applied.

In *Table 2* our results are compared with model calculations of *Schmetz* (1984) in the case of mid-latitude summer model atmosphere for extended area around the Carpathian Basin. The radiation balance values calculated by our method are grouped with respect to different cloud conditions on warm days in September 1991, when the atmospheric conditions were similar to the summer model atmosphere. Homogeneous areas were chosen where the sea and the land surfaces were totally cloudless or covered by extended stratus clouds. From Table 2 it can be seen that there is a good agreement between our results and the model calculated radiation balance values.

Table 2. Surface radiation balance from model calculations and our method

	Clear sky and sea surface	Clear sky and land surface	Cloud of medium thick
Schmetz (1991)	320	290	230
Our method mean values	333	291	226
Variance	4.0	17.6	13.4
N	5	20	26

2.3 Surface temperature

For the determination of the land surface temperature (*LST*) we applied the method of *Prata* (1991):

$$LST = 40 \left[\frac{1-\epsilon}{\epsilon}\right] + \frac{1+\beta}{\epsilon} T_4 - \frac{\beta}{\epsilon} T_5, \tag{8}$$

where

$$\beta = \frac{1-\tau_4}{\tau_4-\tau_5} \tag{9}$$

and all temperature values are in °C.

The channel 4 and 5 transmittances τ_4 and τ_5 were calculated by the radiative transfer model LOWTRAN-7 using TOVS (*TIROS-N Operational Vertical Sounder*) temperature and humidity profiles derived by the *International TOVS Processing Package* (ITPP). ϵ is the average value of the channel 4 and 5 spectral emissivities, which were determined from the 8–14 μm values by the formulae (*Sobrino* and *Caselles*, 1991)

$$\begin{aligned} \epsilon_4 &= \epsilon_{8-14} - 0.003, \\ \epsilon_5 &= \epsilon_{8-14} - 0.001, \end{aligned} \tag{10}$$

whereas the ϵ_{8-14} values were assumed to be linearly related to the vegetation index

$$\epsilon_{8-14} = 0.98 - 0.085 * NDVI. \tag{11}$$

The coefficients for Eq. (11) were determined on the basis of the emissivity data given by *Salisbury* and *Milton* (1988) and from daytime *NDVI* values of agricultural and forested areas in Hungary.

3. *First results*

The accurate knowledge and predictability of the daily amplitude of the active surface temperature (δT) is of primary importance in agriculture. On days without major weather events its magnitude is dependent on the thermophysical properties of the active surface and the daily variation of its energy budget. The total gain of radiant energy during the warming period can well be characterized by the 09 GMT surface radiation balance (R_{09}). On the other hand, investigations (see, for example *Hope* and *McDowell*, 1992) have revealed that there is a linear decrease in the active surface temperature with increasing value of *NDVI*, indicating the relationship between the amount of transpirationally active vegetation and the thermal inertia of the active surface. Hence, these satellite-derived parameters can be good indicators of the daily variation of the active surface temperature. Here the relationship between δT, R_{09} and *NDVI* is investigated over mainly agricultural areas of the Carpathian Basin.

We chose situations when major part of both the afternoon and the previous or following night 1024×1024 pixel NOAA-11 AVHRR images of the Carpathian Basin were found cloud-free by visual interpretation and assumed to be least affected by the disturbing atmospheric effects. At nighttime the cloudy pixels were removed by a thresholding technique using a histogram constructed from the brightness values of channel 4. In the case of the afternoon images the pixels with zero *NDVI* were omitted. Then the brightness temperature and *NDVI* values were averaged over a 16×12 grid with an approximately 20 km spatial resolution.

The investigated area is located in the Great Hungarian Plain (*Fig. 1*), mainly covered with winter and summer crops and forage. We used data of six days from early spring to late autumn representing the whole vegetation period

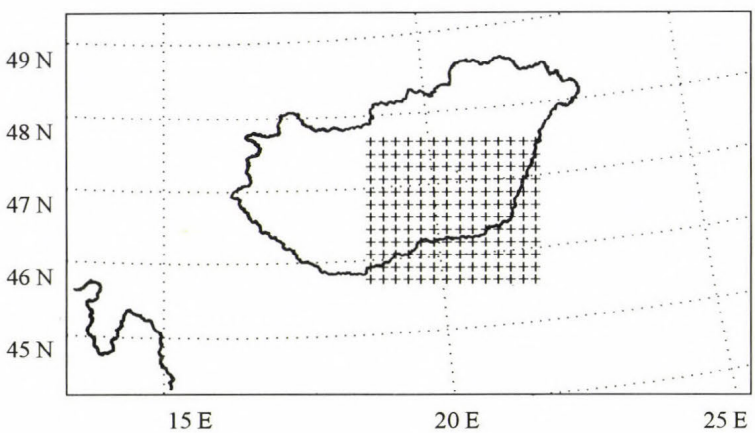

Fig. 1. The geographical area studied.

(*Table 3*). Unfortunately, the years 1992 and early 1993 have been dry and hence are characterized by low *NDVI* values.

Table 3. Dates and case numbers

Date	1992.	20.09	07.11	1993.	10.03	21.04	12.05	02.06
Number		123	18		130	130	115	126

The morning net radiation balance values were calculated from 09 UTC METEOSAT 4 data as described in 2.3. The fields were filtered by spatial coherence calculations. The daily amplitude of the active surface was derived as the difference of the skin temperatures calculated from AVHRR channel 4 and 5 data of the night and afternoon overpasses of the NOAA-11 satellite.

The net radiation at clear sky conditions has small spatial variability over the investigated area. On *Fig. 2* δT data corresponding to separate days form column-like clusters over narrow intervals of net radiation values. This enabled us to investigate the partial effect of the vegetation index. *Fig. 3* illustrates average values of δT corresponding to narrow intervals of *NDVI* on two late spring days. An increasing trend of the temperature amplitude can be observed until the *NDVI* value of 0.25 followed by a decrease due to the evapotranspirational effect of the dense vegetation.

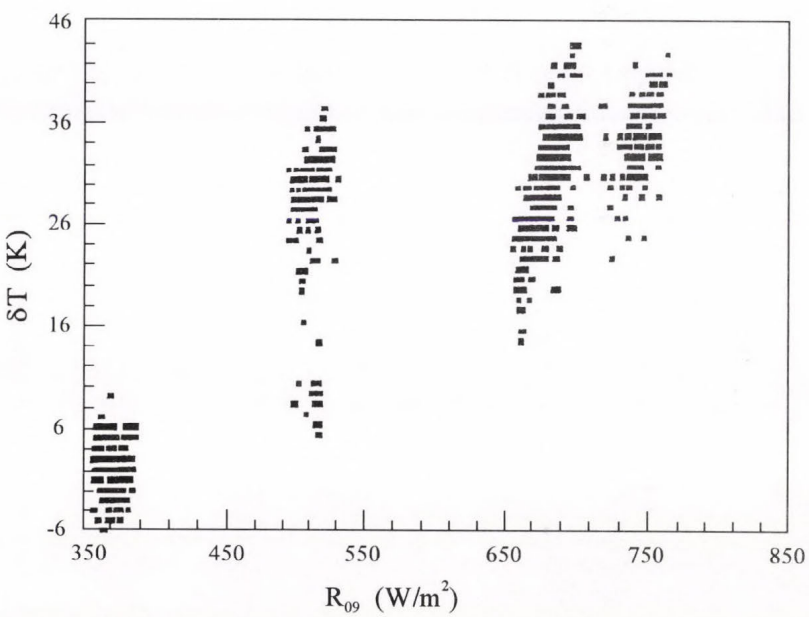

Fig. 2. Variation of δT with R_{09} on the six days studied.

The same phenomenon is shown in *Fig. 4* where data of all the six days have been displayed. It should be noted, however, that in this case the observed

feature is a combined effect of both the *NDVI* itself and the net radiation which has a good correlation with the vegetation index.

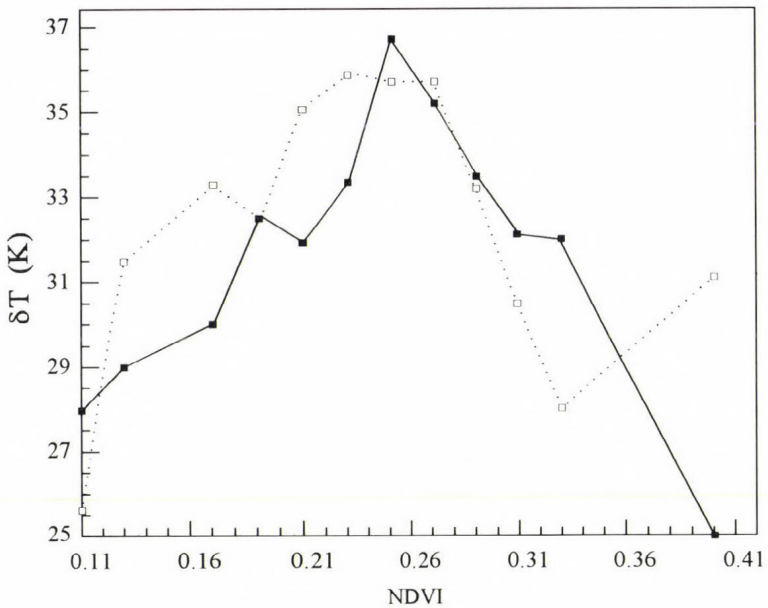

Fig. 3. δT versus *NDVI* on May 12 (solid) and June 2 (dotted).

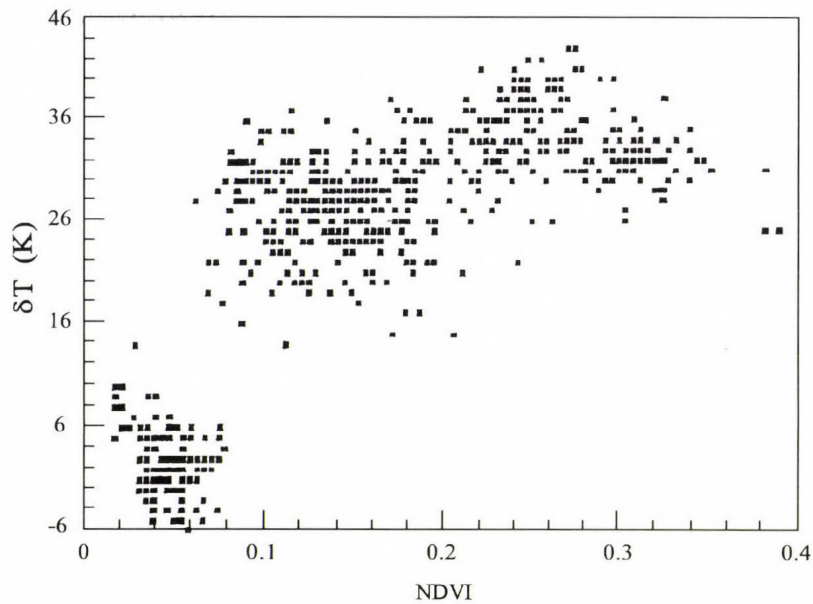

Fig. 4. Variation of δT with *NDVI* on the six days studied.

The partial effect of the net radiation is illustrated in *Fig. 5*. It shows interval-averaged δT as a function of T_{09} corresponding to two intervals of *NDVI*

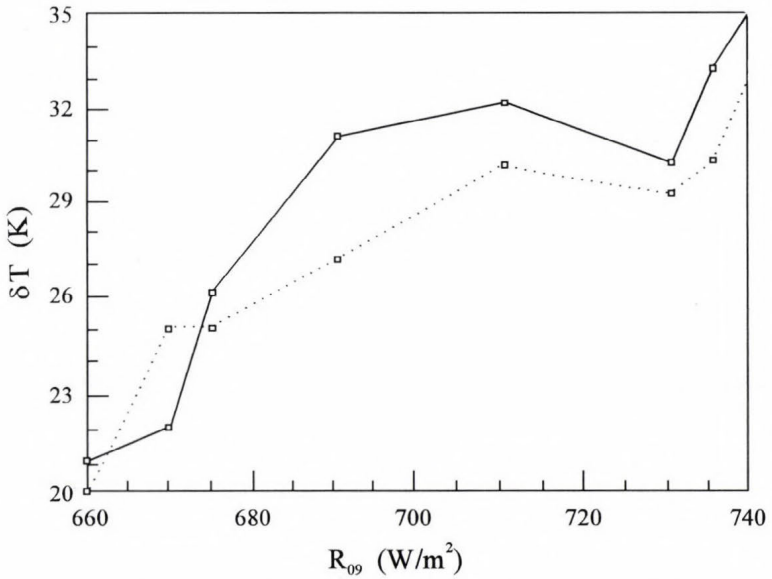

Fig. 5. δT versus R_{09} at $NDVI = 0.20$ (solid) and 0.16 (dotted).

taken from April 21, May 12 and June 2. There is an increase in δT with increasing R_{09}, although this effect on a particular day is small because of the homogeneity of the radiation data.

On *Fig. 6* daily average values of δT, R_{09} and *NDVI* are plotted against the day of the year. The net radiation shows a feature that is determined by the change of the solar height. The annual variation of *NDVI* is characterized by a maximum in late spring and a relatively sharp decrease toward the end of the summer, as it was found by *Derrien et al.* (1992) for agricultural areas simular to the investigated one. On the curve representing δT it can also be seen that the average vegetation index, hardly exceeding the critical value of 0.25 on 12 May could not counteract the increasing effect of the net radiation on the average temperature amplitude.

The above figures indicate that the net radiation is mainly responsable for the annual trend of the daily amplitude of the active surface temperature on which superimposed is a smaller variation caused by the territorial differences of the vegetation index. Thus, to make a quantitative prediction the two parameters have to be taken into account simultaneously.

Therefore, we carried out multiple linear regression calculations. The equation to estimate δT with R_{09} and *NDVI* as independent variables is as follows

$$\delta T = 38.257 * NDVI + 0.05438 * R_{09} - 13.92 . \quad (12)$$

The accuracy of the equation is characterized by a correlation of 0.84 between the observed and predicted δT values.

4. Conclusion and plans

This investigation has shown that the morning net radiation and the vegetation index can be used for the prediction of the daily amplitude of the active surface temperature with an acceptable accuracy. Its annual variation is governed by the net radiation, whereas the territorial differences on a given day are mainly due to the spatial distribution of the vegetation index. The latter has a critical value beyond which the temperature amplitude decreases, indicating the effect of the evapotranspiration of the vegetation.

With the continuous extension of our archive we plan to repeat this study with more data, eliminating the particularities of the chosen days and the dry weather of the investigated period. We plan to use also AVHRR images of the morning NOAA satellites to calculate the net radiation.

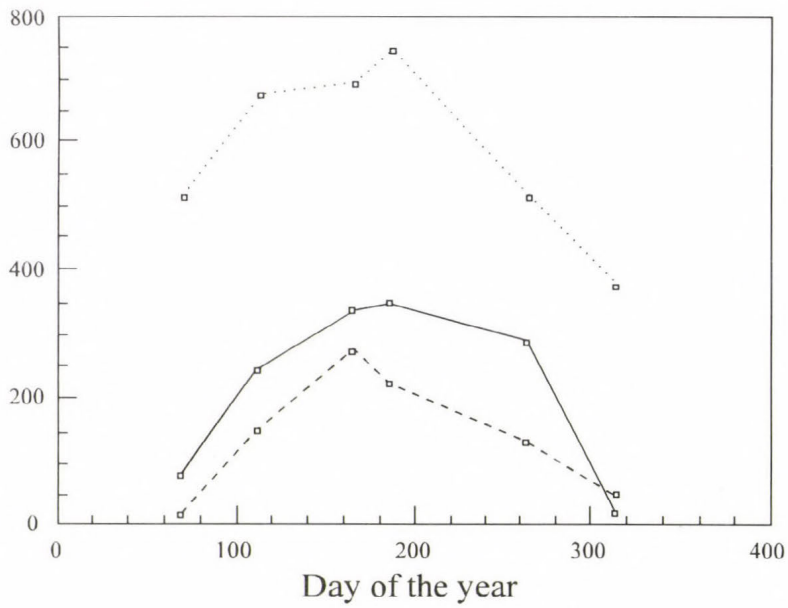

Fig. 6. Annual variation of R_{09} (dotted, W/m^2), δT *10 (solid, K*10) and *NDVI**1000 (dashed).

References

Derrien, M., Farki, B., Le Gléau, H. and *Sairouni, A.*, 1992: Vegetation mapping in 1990 over France using NOAA-11/-AVHRR. *Veille Climatique Satellitaire*, No. 42, 59-67.

Hope, A.S. and *McDowell, T.P.*, 1992: The relationship between surface temperature and a spectral vegetation index of a tall-grass prairie: effects of burning and other landscape controls. *Int. J. Remote Sensing 13*, 2849-2863.

Jackson, R.D., Slater, P.N. and *Pinter, P.J.*, 1983: Discrimination of growth and water stress in wheat by various vegetation indices through clear and turbid atmospheres. *Remote Sensing Environ. 15*, 187-195.

Justice, C.O., Townshend, J.R.G., Holben, B.N. and *Tucker, C.J.*, 1985: Analysis of the phenology of global vegetation using meteorological satellite data. *Int. J. Remote Sensing 6*, 1271-1318.

Kidwell, K. B., 1991: NOAA polar orbiter data users guide. *NOAA National Environmental Satellite, Data and Information Service, National Climatic Data Center Satellite Data Services Division*, Washington, D.C.

Práger, T. and *Kovács, E.*, 1988: Investigation of the climate modifying effects of atmospheric trace gases and aerosol particles by a radiative-convective model. *Időjárás 92*, 153-162.

Prata, F., 1991: Land surface temperature derivation using AVHRR/TOVS. *Technical Proceedings of the Sixth International TOVS Study Conference*, May 1-6, Airlie, Virginia, 401-407.

Rimóczi-Paál, A., 1985: Determination of surface global radiation from METEOSAT images using relative brightness as new parameter to characterize the cloudiness. *Adv. Space Res. 5*, No. 6, 329-332.

Rimóczi-Paál, A., 1989: Relationship between cloudiness and surface global radiation obtained from METEOSAT images. *Adv. Space Res. Vol. 9*, No. 7, 101-104.

Salisbury, J.W. and *Milton, N.M.*, 1988: Thermal infrared (2.5 to 13.5 μm) directional hemispherical reflectance of leaves. *Photogrammetric Engineering and Remote Sensing 54*, 1301-1304.

Schmetz, J., 1984: On the parameterization of the radiative properties of broken clouds. *Tellus 36A*, 417-428.

Schmetz, J., 1991: Retrieval of surface radiation fluxes from satellite data. *Dyn. of Atmosph. and Oceans 16*, 61-72.

Sobrino, J.A. and *Caselles, V.*, 1991: A methodology for obtaining the crop temperature from NOAA-9 AVHRR data. *Int. J. Remote Sensing 12*, 2461-2475.

Tucker, C.J., 1979: Red and photographic infrared linear combination for monitoring vegetation. *Remote Sensing Environ. 8*, 127-139.

Yates, H.W., Tarpley, J.D., Schneider, S.R., McGinnis, D.F. and *Scofield, R.A.*, 1984: The role of meteorological satellites in agricultural remote sensing. *Remote Sensing Environ. 14*, 219-233.

IDŐJÁRÁS

Quarterly Journal of the Hungarian Meteorological Service
Vol. 97, No. 4, October–December 1993

Surface temperature derived from METEOSAT infrared data using atmospheric correction

J. Kerényi

Satellite Research Laboratory, Hungarian Meteorological Service,
P.O. Box 32, H-1675 Budapest, Hungary

(Manuscript received 11 August 1993; in final form 11 November 1993)

Abstract—The brightness temperature of the surface-air system can be determined from the METEOSAT IR window data, but the actual surface temperature cannot be established directly. Therefore a program has been developed to derive the true surface temperature. The brightness temperatures are corrected for effects of water vapour, ozone, uniformly mixed gases and aerosols in the atmosphere, reflected radiation, and sensor filter transmittance. Radiosonde data are used in the applied infrared transmission model. Comparison of satellite derived temperature with the ground measurements show differences of 2–3 degrees at water surface and 1–4 degrees at land surface. This discrepancy can be explained by the difference of two types of measurement methods.

Key-words: METEOSAT, transmittance model, surface temperature.

1. Introduction

A knowledge of surface temperature is strongly required for many applications, notably in agrometeorology, climate and enviromental studies.

The geostationary METEOSAT satellite observes the Earth in three channels in the infrared window (10.5–12.5 μm), in the visible (0.4–1.1 μm) and water vapour absorption band (5.7–7.1 μm).

The longwave radiance can be determined from the brigthness values using the calibration coefficient for METEOSAT. Atmospheric gases absorb energy radiated by the surface, and radiate according to their own temperature, which is typically lower than the surface temperature. Consequently, the radiance detected by satellite is less than the surface radiance and the derived surface temperature will be lower than the ground true value.

The correct temperature of the surface may be estimated by including an atmospheric correction scheme. At the determination of surface temperature the

LOWTRAN 7 transmittance model was used. The model relying on the radiosonde data, determines the longwave radiance at the top of the atmosphere taking into account the effect of the atmosphere. The determination of surface temperature is based on the comparison of the radiances calculated by model and measured by satellite.

Earlier, this method was applied for NOAA by *Irbe et al.* (1979). The water surface temperature was determined by the LOWTRAN 3B transmittance model using the radiosonde and AVHRR data from the NOAA-5.

The difference between the surface and the brightness temperature was investigated by *Tomasi et al.* (1992) using METEOSAT infrared data. At this calculation of the atmospheric correction the LOWTRAN 7 computer programme was applied for a wide set of atmospheric models. The radiance values, simulating the satellite signals and calculated by the model, and the surface temperatures determined in the lack of the atmosphere, were compared. These comparisons and the satellite signals define the value of brightness temperature for each simulated satellite signal, and then the corresponding value of temperature correction equal to the difference between the surface and brightness temperature.

2. Radiosonde data

The atmospheric correction varies with the amount and distribution of attenuators of infrared radiation in the atmosphere, the principal one of which is the water vapour. The calculation of water vapour distribution in the atmosphere was determined from upper air data of two radiosounding stations (Budapest, Szeged) in Hungary. To determine data for other areas of Hungary, a biharmonic spline interpolation was applied. Biharmonic spline interpolation is a special case of the more general multiharmonic spline. The interpolated value at any point of the territory is calculated by superposition of the impact of every measurement point, so the spatial structure of the meteorological field can well be described.

This method was applied for the Carpathian Basin. At the calculation the Hungarian and the neigbourhood radiosonde data (from 8 stations) were used. The interpolation technique produces a pseudo sonde in every gridpoint. Based on the pseudo sondes, the atmospheric transmittance model calculates temperature, humidity and pressure profiles.

3. Atmospheric transmittance model

The atmospheric correction program calculates the transmittance and radiance of the atmosphere from 0 cm^{-1} to 50,000 cm^{-1} at 20 cm^{-1} spectral resolution on a linear wavenumber scale with 5 cm^{-1} sampling.

The LOWTRAN 7 package includes transmittance functions for water vapour, unformly mixed gases and ozone, and absorption coefficients for the gaseous elements and aerosols.

In the present application, calculations are limited to the 800–950 cm^{-1} channel of the sensors on board METEOSAT.

The thermal radiation leaving the Earth's atmosphere at radiometer altitude and measured through a filter system can be formulated by the radiative transfer equation. The detected radiance consists of the surface emitted radiation, the reflected radiation and the radiation emitted by the atmosphere, respectively

$$N(Z,u) = \frac{1}{\pi}\int_{\nu_1}^{\nu_2} \phi(\nu)\varepsilon(\nu)B_\nu(T_0)t_\nu(0,Z,u)d\nu +$$

$$+\frac{1}{\pi}\int_{\nu_1}^{\nu_2}\int_{0}^{Z} \phi(\nu)(1-\varepsilon(\nu))t_\nu(0,Z,u)B_\nu(T(z))\frac{\partial t_\nu(0,z,u)}{\partial z}dzd\nu +$$

$$+\frac{1}{\pi}\int_{\nu_1}^{\nu_2}\int_{0}^{Z} \phi(\nu)B_\nu(T(z))\frac{\partial t_\nu(z,Z,u)}{\partial z}dzd\nu, \qquad (1)$$

where the following notation are used: $N(Z,u)$ detected radiance, θ zenith angle, u cos θ, Z satellite altitude, υ wave number, $\Phi(\upsilon)$ normalized response function, $B_\upsilon(T)$ Planck function at absolute temperature T, $\epsilon(\upsilon)$ emissivity of the radiating surface, T_0 surface temperature, $t_\upsilon(z_1,z_2,u)$ transmittance of the layer located between altitudes z_1 and z_2 for incidence θ and

$$t_\nu(z_1,z_2,u) = \exp\left(-\frac{1}{u}\int_{z_1}^{z_2} K_\nu(z)dz\right), \qquad (2)$$

where K_υ is the total absorption coefficient which is equal to sum of the aerosol and molecular absorption coefficient.

Formally integrating the radiative transfer equation along the atmospheric path, the upwelling infrared radiance at each wavelength measured by a satellite borne radiometer is given by the sum of the following three terms: (1) the surface contribution, depending on surface spectral emittance (also called emissivity), surface temperature and atmospheric transmittance; (2) the atmospheric contribution, which is given by the integral along the whole atmospheric path of the radiance emitted by each infinitesimal element of air volume attenuated by the overlying atmosphere; and (3) the contribution of the infrared radiation emitted downwards by the atmosphere and reflected by the surface. Therefore, the first contribution gives direct information about surface

temperature on the basis of the black-body theory; the second contribution partly compensates the loss of surface radiance caused by atmospheric attenuation; and the third contribution depends mainly on the surface reflection of downwelling infrared radiance, so it decreases as emittance increases and can be consequently neglected in all cases in which surface emittance is very close to unity at all wavelenghts. Since the second term, due to the atmospheric emission, masks the surface contribution, the apparent brightness temperature differs from surface temperature, in general.

The LOWTRAN model is used to calculate the transmittance including in (1), the normalized response function is incorporated into the program, and the emissivity is assumed to be unity in every case.

4. Determination of surface temperature by model

Since the surface temperature cannot be established directly from radiance measured by satellite, the LOWTRAN 7 model is applied. The model, using the pseudo sondes, determines the longwave radiance at the top of atmosphere.

The radiance measured by satellite and the data calculated by model were compared, and the measured values were grater than the calculated data. A reason for these deviations may be the fact that the model doesn't use the surface temperature itself, but rather value measured by the radiosonde near the surface. In order to accomplish this procedure, it is assumed that the calculated and the measured radiances are equal. An iteration method was employed for determining the near-surface temperature. The starting point was increased by 0.25 degrees, then the model calculated the longwave radiance using the corrected temperature. This procedure was continued until the difference between the measured and the calculated radiance values was less than the required precision. The temperature determined by the iteration method represents the actual surface temperature.

At the calculation TEMP measured at 12 UTC was used. The radiance measured by satellite was determined from the METEOSAT-4 infrared pictures received at 11 or 12 UTC.

5. Results

The emissivities were assumed to be unity in every case. This assumption is best for water and snow surfaces, therefore these surfaces were investigated first. For actual soil and vegetated surfaces the assumed emissivity may be incorrect and we have to estimate its value to calculate accurate temperatures. An error of only 1% in emissivity causes about 1K error in the determination of surface temperature. However, if the emissivity is equal to unity, the surface temperature will be underestimated.

One area examined was Lake Balaton and the temperature calculation was performed in clear weather in all cases. A gridpoint is near the Siófok Observatory where temperatures measured by resistance thermometer are available for comparison. The measured values, the brightness temperatures determined from the IR counts and the surface temperatures calculated with atmospheric correction scheme are shown for Balaton during 1992 in *Fig. 1.*

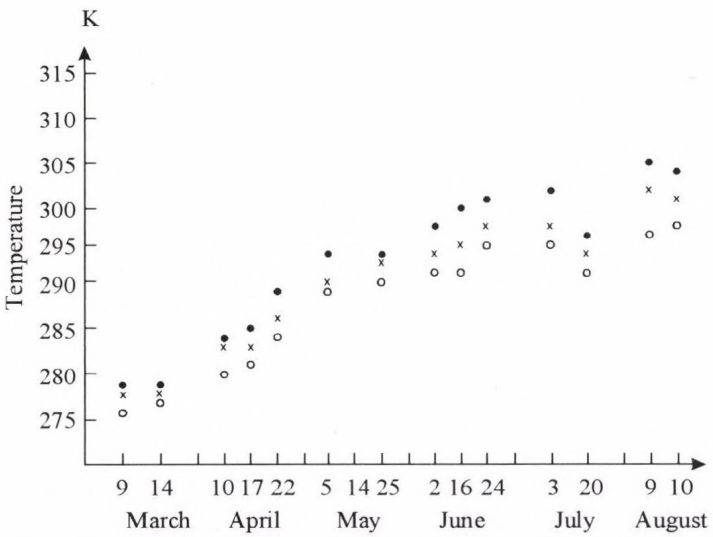

Fig. 1. Temperature values of Lake Balaton (denotations: × — measured temperatures, o — brightness temperatures, • — surface temperatures with atmospheric correction).

The calculated temperatures values were typically 2–3K lower, while the corrected temperatures were 2–3K greater than the measured water temperatures, which were confirmed by measurements (*Péczely*, 1974). The measurements showed, that the difference between the temperatures of water surface and lower layer (2 m) were around 2 degrees in the early afternoon. A possible reason for the difference is that the measurement is performed at only point, whereas the satellite temperatures are averaged over large areas, and the other reason may be that the measurement at the observatory is carried out in depth of 1.5 m, while the calculated temperature can be considered to be the skin temperature.

The region of Szarvas Agrometeorology Observatory was chosen for the other investigation, because it is situated in lowland territory and near the Szeged radiosonde station. Comparing the measured (mercury thermometer) and calculated temperatures, the calculated values were also lower than the measured data, as shown in *Fig. 2.*

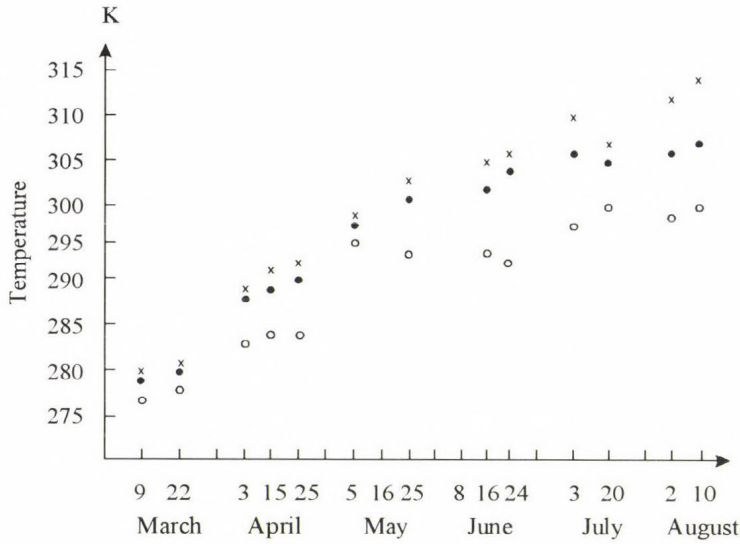

Fig. 2. Temperature values of land station, Szarvas (denotations are the same as in Fig. 1).

The early spring surface temperatures agree within 1–2K, but the differences increase gradually with the growth of vegetation, to 4–5K in summer. If the emissivity is unity, the calculated surface temperature will be lower. The difference between the calculated and measured temperatures can be partly explained by different emissivities of the surfaces in the examined region. The satellite measurements give average values, which are typical to the totality of surfaces. On the other hand, the surface temperatures are measured in one point on bare soil in Szarvas.

6. Summary

Summarizing the conclusions of the investigation, it can be stated, that on the basis of METEOSAT digital images using the radiative-transfer model, the surface temperature can be determined. The results obtained so far are promising for the future in spite of the existing deviations. In case of Lake Balaton, the difference between the measured and the calculated temperature is no more than 2–3K, which derives from the dissimilarity of the two types of measurements. At the land surface of Szarvas in early spring, the temperature difference was only 1–2K, although the difference increased with the growth of plants, due to neglecting emissivity and the different measuring method.

In the future, the determination of surface temperature will be made better, if the variation of emission will also be taken into account.

References

Irbe, G.J., Morcette, J.J. and *Hogg,W.D.*, 1979: Surface water temperature of lakes from satellite infrared data corrected for atmospheric attenuation. Canadian Climate Centre. *Report* No. 79-7.

Tomasi, C., Vitale, V. and *Bencivenni, S.*, 1992: Calculations if the atmospheric correction terms for surface temperature measurements from METEOSAT infrared data. *Proceedings of 9th METEOSAT Scientific User's Meeting*. Locarno, Switzerland, 15-18 September, pp. 369-375.

Péczely, Gy., 1974: *Climate of Lake Balaton* (ed.: B. Béll and L. Takács) (in Hungarian). Országos Meteorológiai Szolgálat Hivatalos Kiadványa, Budapest.

IDŐJÁRÁS

Quarterly Journal of the Hungarian Meteorological Service
Vol. 97, No. 4, October–December 1993

Surface temperature as an important parameter of plant stand

A. Anda

Pannon Agricultural University of Keszthely,
P.O. Box 71, H-8361 Keszthely, Hungary

(Manuscript received 16 September 1993; in final form 24 November 1993)

Abstract—Plants of diverse genetic origin may respond differently to the same environment. Our objective was to assess response of three different sugar beet varieties to the growing season drought during 1992, as inferred from surface temperatures (soil and foliage) and stomatal resistances. Together with diffusive resistance both the soil and foliage temperatures measured by infrared thermometer were sensitive indicators of plant physiological processes and production of sugar beet during the whole measuring period. Significant differences in such parameters as surface temperature and stomatal resistances of sugar beets of various genetic origin appeared only about solar noon. At low angle of solar radiation incidence there was no significant difference in temperature and resistance among the three beet cultivars. Because of well-known advantages of infrared thermometers (quickness and repeatability), they seem to have primary importance in comparative studies, mainly in such investigations where the number of treatments is generally high. In practice, one of this research areas is the plant breeding.

Key-words: canopy and soil temperatures, stomatal resistance, sugar beet varieties, LAI, sugar yield.

1. Introduction

Description and characterization of physiological properties of plant varieties is desirable, and provides a basis for the selection of the best genotype by plant breeders. Response of plants to their surrounding environment also involves interaction between genotypes and environment. One considers these responses when selecting the best genotype to respond under both favourable and non-favourable weather (*Hattendorf et al.*, 1990).

Similar to other plant species, in sugar beet stands water deficit caused stomatal closure (increased resistance and decreased transpiration) and rose canopy foliage temperature (*Brawn* and *Rosenberg*, 1970; *Lawlor* and *Milford*, 1975; *Huzulak* and *Matejka*, 1992). Determination of plant surface temperature

in assessing water status of plants has become quite common (*Pinter et al.*, 1979; *Idso et al.*, 1981; *Jackson*, 1982; *Keener* and *Kirchner*, 1983; *Walker* and *Hatfield*, 1983; *Tubaileh et al.*, 1986; *Smith et al.*, 1988; *Hattendorf et al.*, 1990). Infrared thermometers are often used to measure canopy foliage temperature because they provide precise and quick measurements and allow numerous nondestructive readings (*Halim et al.*, 1991). In plant breeding, the quickness has primary importance because the numerous treatments (plant cultivars) require instantaneous sampling. Many studies exist dealing with the use of plant surface temperature in determining plant physiological processes (mainly transpiration), but there is little information available on the importance of soil surface temperature, an important regulator of plant water loss.

Previous research has mostly characterized crop response to soil water deficit through the use of canopy surface temperature (*Mtui et al.*, 1981). The research reported here was devoted to an evaluation of the utility of both canopy and soil surface temperature measurements as quick indicators of plant response to surroundings. A means for evaluating temperature, the main cause of plant physiological processes could open the way to improved selection of varieties of different genetic origin that could ultimately lead to better yield production.

2. Experimental procedure

Field trials were conducted at Keszthely Agrometeorological Research Station during the growing season in 1992. Three sugar beet varieties of different genetic origin were planted in 4 m^2 plots (split-block design) with four repetitions on a Ramann type brown forest soil. The variety *Kawemaya* is the most frequent grown sugar beet cultivar in Western Europe. Originally, it was bred in Germany. The other two varieties, *Gála* and *Éva*, are breeding in Hungary. The plant population ranges between 10 and 12 plants per m^2.

Leaf area was measured by a LI-3000 type portable planimeter on 5 plants in each treatment every two weeks after emergence. Stomatal resistance was estimated with LI-60 type diffusive porometer on the exposed upper leaves with three to five repetitions. As significant differences in resistances of different sugar beet varieties occurred at high angles of solar radiation incidence only, these results will be presented as surface temperature measurements.

Canopy temperature readings – similar to those of soil surface temperature – were taken about solar noon each day when the radiation was undisturbed (clear sky conditions). At canopy temperature determinations the RAYNGER II.RTL type infrared thermometer was hand held at about 1 m above the canopy using an oblique angle of about 30°. In these cases, the sampling time was 30 seconds with three repetitions in each treatment. The average canopy temperature was calculated from temperature readings. The field of view of the instruments is 8°, the emissivity was assumed to be 0.98.

Because of the well-known heterogeneity of soil temperature measured by traditional mercury thermometers, soil surface temperature was measured with an infrared thermometer. This instrument takes 4 samples per second. The entire surface area of each plot was sampled by carrying the thermometer about 10 cm above the soil surface between the plant rows. From these readings, the surface temperature represented the average of the entire plot.

At the end of vegetative period, the sugar yield was determined by measuring both the root yield and sugar content of each sugar beet varieties.

3. Results and discussion

3.1 Assimilatory surface

The effect of change in plant biomass is twofold: the direct influence on size of photosynthetic area, and the indirect effect of plant architecture on canopy microclimate. The assimilatory surface can be therefore characterized easily by *leaf area index* (LAI).

There was no significant difference in LAI of sugar beet varieties in the first half of investigative period (from the middle of May to the end of June) when the weather was not dry and hot (*Fig. 1*). But as the drought in July occurred, the LAI curves of different beet cultivars separated. The largest assimilatory surface appeared in Kawemaya's canopy, where the size of LAI was almost two

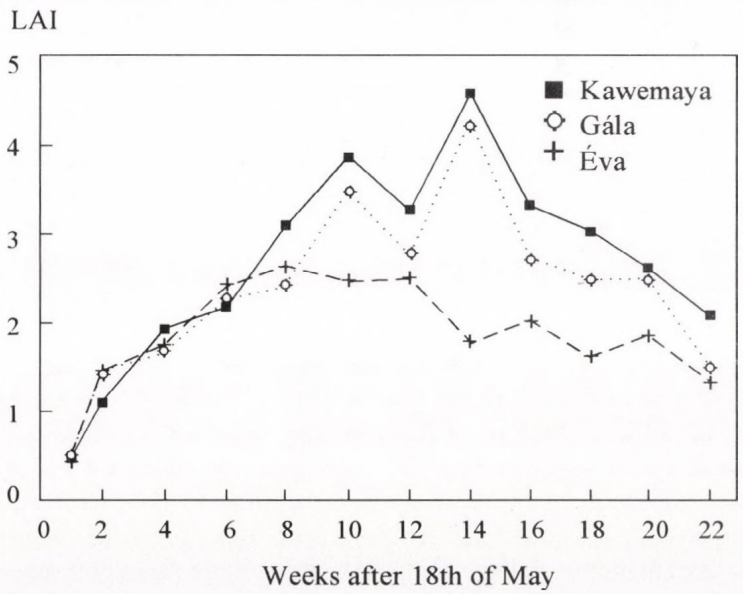

Fig. 1. Seasonal variation of leaf area index in 1992.

times higher than that of the LAI of Éva, the cultivar of lowest green area. Results of Gála were between the LAI of Kawemaya and Éva, but closer to the leaf area of Kawemaya.

4. Soil surface temperature

In May and June, when the LAI of the three beet varieties was nearby identical, the soil surface temperature of Kawemaya's plots increased significantly (*Fig. 2*). From the end of July, the higher the size of assimilatory surface, the cooler the soil surface temperature. Increased LAI of Kawemaya resulted in a 3 to 4°C decrease in instantaneous soil surface temperature compared to the values of Éva, the beet cultivar with the smallest assimilatory surface.

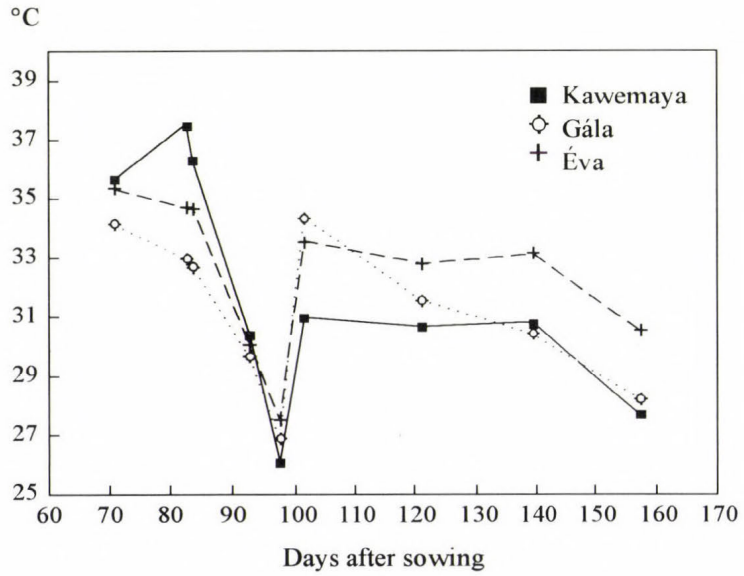

Fig. 2. Soil surface temperature about solar noon, 1992.

5. Canopy temperatures

There was little difference in plant canopy temperatures between the three varieties until the end of July (*Fig. 3*). Coincident with drought in August 1992, the canopy temperature curves separated according to the direction of change in soil temperatures. Coolest soil temperatures coincided with the treatment of the lowest instantaneous foliage temperature readings (Kawemaya).

The foliage temperature of Éva, the warmest treatment of the 3 varieties, was 3 to 6.5°C higher than the surface temperature of Kawemaya during the

dry and hot August of 1992. The degree of change in plant temperature seems to be high enough to modify the main plant physiological processes (photosynthesis, respiration and transpiration) and the production of dry matter.

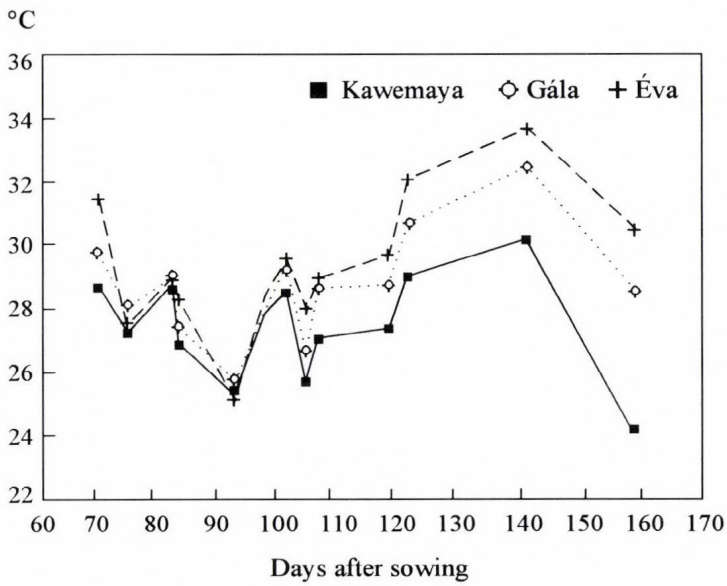

Fig. 3. Canopy temperature about solar noon, 1992.

6. Stomatal resistance

Independent of sugar beet cultivar, the instantaneous resistances measured at high incidence of solar radiation were two to three times larger than those resistance values determined earlier in the growing season. The likely explanation might be the occurrence of drought during the investigated period of 1992.

Hall et al. (1988) and *Mtui et al.* (1981) pointed out that difference in genotypes had no effect on stomatal conductances of alfalfa and corn varieties. In contrast, *Hattendorf et al.* (1990) found significant differences in stomatal conductance and water use efficiency among alfalfa cultivars with diverse origins.

In our study, there was a significant difference in stomatal resistances of different beet varieties during the dry and hot investigation period of 1992 (*Fig. 4*). The lowest resistances occurred in Kawemaya's canopy resulting in the largest transpiration and water losses. Mainly in the first half the data collection period Éva had larger stomatal resistances than the other two cultivars. As resistance decreases the pores open and the transpirational cooling is greater. It was concluded that soil temperature was one of the most important regulators

(driving force) of transpiration. At higher soil temperatures, transpiration intensity increases. In our study an opposite tendency occurred: the variation of warmest soil temperature and greatest stomatal resistance was the same (the cultivar Éva). The likely reason might have been the drought of 1992 growing season. Stomatal resistance of Kawemaya was the lowest, when the soil surface temperature was the coolest.

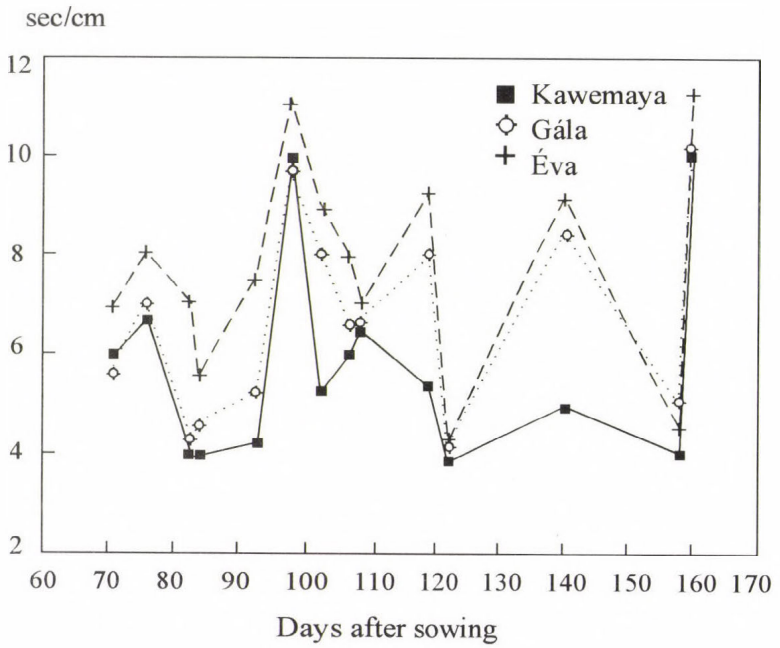

Fig. 4. Production of sugar beet varieties of diverse genetic origin.

7. Production of plants

In assessing sugar beet yield, two elements of yield, root mass and sugar content must be considered (*Fig. 5*). During the 1992 growing season, the variety Gála had the largest root yield of all. Decrease in root yield of Kawemaya and Éva were 8.1 and 36.7%, respectively compared to Gála.

There was no significant difference in sugar content between cultivars of Gála and Éva. The sugar percentage of Kawemaya increased by 10.2 and 10.3% compared to the sugar ratio of Gála and Éva varieties, respectively.

The goal of sugar beet production is to achieve the highest amount of produced sugar per unit area of soil. The cultivar with the highest production was Kawemaya. Decreases in sugar yield were 34.6 and 40.3% in Gála and Éva respectively, compared to Kawemaya.

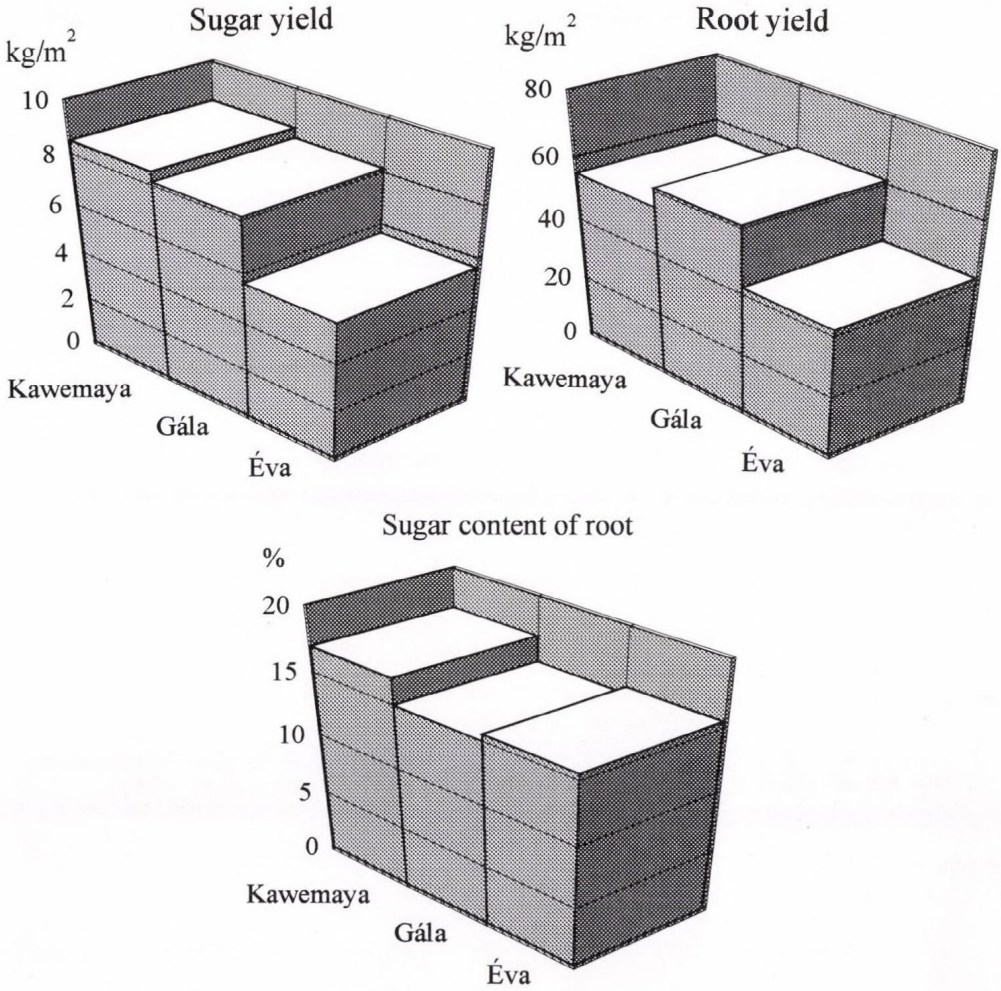

Fig. 5. Production of different sugar beet varieties.

The plant canopy and soil temperatures, and stomatal resistances were the most favourable in Kawemaya's canopy during the growing season in 1992. The greater sugar yield of the Kawemaya seems to be related to higher assimilatory surface resulting in an increased ability to produce more photosynthate. The greater biomass shadowed soil moderating soil surface temperature. At lower soil temperature the stomatal resistances decreased as transpiration increased. The cooler foliage temperature caused by low resistance values in Kawemaya's stand indicates greater transpirational cooling. In similar situations, one observes greater photosynthesis and subsequently greater yield (*Tanner* and *Sinclair*, 1981). Results of sugar production agree well with earlier investigations of *Sinclair et al.* (1981).

In our experiment, both canopy temperature and stomatal resistance values provided satisfactory results studying differences in parameters of sugar beet varieties of diverse genetic origin. As opposed to *Mtui et al.* (1981) stomatal resistance was as sensitive as canopy temperature, when non-irrigated field trial was carried out. Because of quickness of infrared thermometers, the canopy temperature seems to be a better indicator when assessing alterations of different plant varieties. The porometer use in comparative studies is time consuming, and since it is a point measurement, very uncertain. In contrast to stomatal resistance determinations, at infrared thermometer use the repeatability of temperature measurement is practically unlimited. In comparative studies (in plant breeding), when numerous treatments are investigated, the canopy temperature determinations should have primary importance. In our experiment, canopy temperature was sensitive indicator of physiological properties of sugar beet cultivars of diverse genetic origin. In practice, surface temperature measurements could serve a quick up-to-date method for plant breeders in selection of (sugar beet) varieties.

References

Brawn, K.W. and *Rosenberg, N.J.* 1970: Influence of leaf age, illumination, and upper and lower surface differences on stomatal resistance of sugar beet leaves. *Agron. J. 62*, 20-24.

Halim, R.A., Buxton, D.R., Hattendorf, M.J. and *Carlson, R.E.*, 1991: Crop water stress index and forage quality relationships in alfalfa. *Agron. J. 82*, 906-909.

Hall, H.M., Sheaffer, C.C. and *Heidel, G.H.*, 1988: Partioning and mobilization of photoassimilate in alfalfa subjected to water deficit. *Crop Sci. 28*, 964-969.

Hattendorf, M.J., Evans, D.W. and *Peaden, R.N.*, 1990: Canopy temperature and stomatal conductance of water stressed dormant and non-dormant alfalfa types. *Agron. J. 82*, 873-877.

Huzulak, J. and *Matejka, F.*, 1992: Stomatal resistance, leaf water potential and hydraulic resistance of sugar beet plants. *Biologia Plantarum 34*, No. 3-4, 291-296.

Idso, S.B., Reginato, R.J., Reicosky, D.C. and *Hatfield, J.L.* 1981: Determining soil-induced plant water potential depressions in alfalfa by means of infrared-thermometry. *Agron. J. 73*, 826-830.

Jackson, R.D., 1982: Canopy temperature and crop water stress. *Adv. in Irrig. 1*, 43-85.

Keener, M.E. and *Kirchner, P.L.*, 1983: The use of canopy temperature as an indicator of drought stress in humid regions. *Agric. Met. 28*, 339-349.

Lawlor, D.W. and *Milford, F.J.*, 1975: The control of water and carbon dioxid flux in water stressed sugar beet. *J. Exp. Botany 26*, 657-665.

Mtui, T.A., Kanemasu, E.T. and *Wassom, C.*, 1981: Canopy temperature, water use, and water use efficiency of corn genotypes. *Agron. J. 72*, 456-458.

Pinter, P.J. Jr., Stanghellini, M.E., Reginato, R.J., Idso, S.B., Jenkins, A.D. and *Jackson, R.D.*, 1990: Remote detection of biological stresses in plants with infrared thermometry. *Science 205*, 585-587.

Tanner, C.B. and *Sinclair, T.R.*, 1981: Efficient water use in crop production: Research or re-search. In *Efficient Water Use in Crop Production* (eds.: T.R. Sinclair, H.M. Taylor and W.R. Jordan). Amer. Soc. of Agron., Madison, Wisconsin.

Smith, R.C.G., Barrs, H.D. and *Fischer, R.A.*, 1988: Inferring stomatal resistance of sparse crops from infrared measurements of foliage temperature. *Agric. and For. Meteorol. 42*, 189-198.

Tubaileh, A.S., Sammis, T.W. and *Lugg, D.G.*, 1986: Utilization of thermal infrared thermometry for detection of water stress in spring barley. *Agric. Water Manag. 12*, 75-85.

Walker, G.K. and *Hatfield, J.L.*, 1983: Stress measurements using foliage temperature. *Agron. J. 75*, 623-629.

BOOK REVIEWS

H. B. Bluestein: **Synoptic-Dynamic Meteorology in Midlatitudes**. Vol. I: **Principles of Kinematics and Dynamics**. Oxford University Press, 1992, 431 pages; Vol. II: **Observations and Theory of Weather Systems**. Oxford University Press, New York, Oxford, 1993, 594 pages.

More than thirty years have elapsed since the publishing of the last edition of the two-volume textbook in synoptic meteorology by *Professor Sverre Petterssen* (*Weather Analysis and Forecasting*, Second Edition, Vol. I and II, McGraw-Hill, New York, 1956). The work of *Professor Howard B. Bluestein* provides a modern, updated replacement of the classical textbook of *S. Petterssen*. No other summarizing work has been published in synoptic meteorology since the middle of the fifties, meanwhile a series of good textbooks appeared in dynamic meteorology in the last three decades (e.g. *J.R. Holton*: *An Introduction to Dynamic Meteorology*, Third Edition, 1992; *A.E. Gill*: *Atmosphere-Ocean Dynamics*, 1982; *J.A. Dutton*: *The Ceaseless Wind*, 1986; *H. Pichler*: *Dynamics of the Atmosphere* (in German), 1984; *G.J. Haltiner* and *R.T. Williams*: *Numerical Prediction and Dynamic Meteorology*, Second Edition, 1980; *E. Palmén* and *C.W. Newton*: *Atmospheric Circulation Systems*, 1969).

This new, comprehensive textbook presents essential information about modern weather forecasting and analysis. It is based on *Professor Bluestein*'s fifteen years of teaching experience at the University of Oklahoma. *Professor Bluestein* received B.S. and M.S. degrees in electrical engineering and M.S. and Ph.D. degrees in meteorology from the Massachusetts Institute of Technology, he is a former *Oklahoma Professor of the Year*, and a recipent of the *Regents' Award for Superior Teaching*.

Vol. I of the book carefully examines the foundations of synoptic meteorology, from the analysis of scalar fields to atmospheric kinematics, dynamics and thermodynamics. Contemporary topics such as Q-vectors, and modern observing systems such as Doppler radar and lidar are discussed and the work emphasizes both physical understanding and mathematical analysis, and clearly explains observations in light of current theory.

Vol. II covers the interpretation of the behaviour of synoptic-scale systems in the context of both quasi-geostrophic theory in pressure coordinates and isentropic potential vorticity analysis. Frontal theory and observations are encompassed, along with mesoscale phenomena such as the coastal front, the dryline, and fronts that behave like trapped gravity currents. Semi-geostrophic theory, symmetric instability and jets are also detailed. Supercells, ordinary cells, mesoscale convective complexes, tornadoes, hail and microbursts are

discussed in the context of their larger scale environment. The text includes many helpful figures, photographs, selected problems and useful references for further readings.

This new, major textbook can be recommended for both undergraduate and graduate students of meteorology, workers of the weather forecast centres and for students of the new university postgraduate schools starting this year.

Gy. Gyuró

S. S. Butcher, R. J. Charlson, G. H. Orians and *G. W. Wolfe* (eds.): **Global Biogeochemical Cycles**. Academic Press, London, San Diego, New York, Boston, Sydney, Tokyo and Toronto, 1992. International Geophysical Series, Vol. 50, 367 pages.

During the last decade a new branch of sciences has been developed: the environmental science. In classical sense this science has a multidisciplinary character. However, the most important feature of this new science is that it wants to study the Nature as a global entity and does not bother with old classification of natural sciences. One of the main reasons for the development of this new discipline is the influence of mankind on our environment which has formed in close relationship with the biosphere during geological times. The most important subject area of environmental science is to investigate the huge material flow in Nature called the biogeochemical cycles.

The main aim of the present book is to discuss in one volume our knowledge of this essential field. The authors, coming from different research areas from biology to atmospheric science, try to summarize what we know about "the transport and transformation of substances in the natural environment, as seen in global context". The book is composed of sixteen chapters. After a short introduction the evolution of the Earth and the biosphere is presented. In two chapters the modeling of biogeochemical cycles and the chemical bases (e.g. equilibria, reaction rates) necessary for the study of the cycles are outlined. A separate chapter deals with tectonic processes playing an important role in shaping our planete. Then come four chapters discussing separately the pedosphere, the sediments, the ocean and the atmosphere. The next five chapters are devoted to a concise presentation of the biogeochemical cycles of such basic species like carbon, nitrogen, sulfur, phosphorus and different metals. The volume is closed with the discussion of human modification of global biogeochemical cycles.

Even this short enumeration shows the importance of this book. It should be added that these important subjects are treated in a fascinating way by the authors working mostly at the University of Washington (Seattle, WA, U.S.A.)

and the University of Stockholm (Sweden). Thus, they are congratulated for doing this not easy job. It goes without saying that some details in the text can be disputed. However, this does not touch the main merits of this work which is unique in this field. Different people can see differently the same subject. Briefly speaking, the use of this book is highly recommended to all scientists dealing with the study of biogeochemical cycles of different elements or compounds in the environment. It can be useful in particular for graduate students who want to get a specialization in environmental science.

E. Mészáros

ATMOSPHERIC ENVIRONMENT

an international journal

To promote the distribution of Atmospheric Environment *Időjárás* publishes regularly the *contents* of this important journal. For further information the interested reader is asked to contact *Dr. P. Brimblecombe,* School for Environmental Sciences, University of East Anglia, Norwich NR 7TJ, U.K.

Volume 27A Number 13 1993

Volume 27A Number 14 1993

R.T. McNider, M.P. Singh and *J.T. Lin*: Diurnal wind-structure variations and dispersion of pollutants in the boundary layer, 2199-2214.

P.M. Midgley and *D.A. Fisher*: The production and release to the atmosphere of chlorodifluoromethane (HCFC 22), 2215-2223.

A.J. Hayter and *M.M. Dowling*: Experimental designs and emission rate modeling for chamber experiments, 2225-2234.

Short Communication

G. Tidy and *J.N. Cape*: Ammonia concentrations in houses and public buildings, 2235-2237.

J. Padro, K.J. Puckett and *D.N. Woolridge*: The sensitivity of regionally averaged O_3 and SO_2 concentrations to ADOM dry deposition velocity parameterizations, 2239-2242.

Volume 27A Number 15 1993

G.J.H. Roelofs: A cloud chemistry sensitivity study and comparison of explicit and bulk cloud model performance, 2255-2264.

S.R. Hanna, J.C. Chang and *D.G. Strimaitis*: Hazardous gas model evaluation with field observations, 2265-2285.

A. Singer, Y. Shamay, M. Fried and *E. Ganor*: Acid rain on Mt Carmel, Israel, 2287-2293.

Xiaoming Zhang and *A.F. Ghoniem*: A computational model for the rise and dispersion of wind-blown, buoyancy-driven plumes-I. Neutrally stratified atmosphere, 2295-2311.

R.S. Thompson: Building amplification factors for sources near buildings: a wind-tunnel study, 2313-2325.

J.W. Spence, F.W. Lipfert and *S. Katz*: The effect of specimen size, shape, and orientation on dry deposition to galvanized steel surfaces, 2327-2336.

J. Baron and *A.S. Denning*: The influence of mountain meteorology on precipitation chemistry at low and high elevations of the Colorado Front Range, U.S.A., 2337-2349.

M. van Loon: Testing interpolation and filtering techniques in connection with a semi-Lagrangian method, 2351-2364.

S.J. Harrison, J.A. Vale and *C.D. Watts*: The estimation of aerial inputs of metals to estuarine waters from point pattern data using an isoplething technique: Severn Estuary, U.K., 2365-2373.

I.P. Bibby, G. Poots and *P.L.I. Skelton*: Theoretical aspects of iceload measurements on fixed rods and overhead line conductors: a transfer function for dry rime-ice accretion, 2375-2383.

I.M. Madany and *S. Danish*: Spatial and temporal patterns in nitrogen dioxide concentrations in a hot desert region, 2385-2391.

F. Fortezza, V. Strocchi, G. Giovanelli, P. Bonasoni and *T. Georgiadis*: Transport of photochemical oxidants along the northwestern Adriatic Coast, 2393-2402.

Volume 27A Number 16 1993

The Russian/American Desert Dust Experiment (Tadzhikistan) 1989

IDŐJÁRÁS

VOLUME 97 * 1993

BUDAPEST, HUNGARY

AUTHOR INDEX

TABLE OF CONTENTS

I. Papers

II. Book review

III. News

Contents of journal Atmospheric Environment, 1993

IV. SUBJECT INDEX

The asterisk denotes book reviews

NOTES TO CONTRIBUTORS

The purpose of *Időjárás* is to publish papers in the field of theoretical and applied meteorology. These may be reports on new results of scientific investigations, critical review articles summarizing current problems in certain subject, or shorter contributions dealing with a specific question. Authors may be of any nationality but papers are published only in English.

Papers will be subjected to constructive criticism by unidentified referees.

* * *

The manuscript should meet the following formal requirements:

Title should contain the title of the paper, the names(s) of the author(s) with indication of the name and address of employment.

The title should be followed by an *abstract* containing the aim, method and conclusions of the scientific investigation. After the abstract, the *key-words* of the content of the paper must be given.

Three copies of the manuscript, typed with double space, should be sent to the Editor-in-Chief: *P.O. Box 39, H-1675 Budapest,* Hungary.

References: The text citation should contain the name(s) of the author(s) in Italic letter or underlined and the year of publication. In case of one author: *Miller* (1989), or if the name of the author cannot be fitted into the text: *(Miller,* 1989); in the case of two authors: *Gamov* and *Cleveland* (1973); if there are more than two authors: *Smith et al.* (1990). When referring to several papers published in the same year by the same author, the year of publication should be followed by letters a,b etc. At the end of the paper the list of references should be arranged alphabetically. For an article: the name(s) of author(s) in Italics or underlined, year, title of article, name of journal, volume number (the latter two in Italics or underlined) and pages. E.g. *Nathan, K. K.,* 1986: A note on the relationship between photosynthetically active radiation and cloud amount. *Időjárás 90,* 10-13. For a book: the name(s) of author(s), year, title of the book (all in Italics or underlined with except of the year), publisher and place of publication. E.g. *Junge, C. E.,* 1963: *Air Chemistry and Radioactivity.* Academic Press, New York and London.

Figures should be prepared entirely in black India ink upon transparent paper or copied by a good quality copier. A series of figures should be attached to each copy of the manuscript. The legends of figures should be given on a separate sheet. Photographs of good quality may be provided in black and white.

Tables should be marked by Arabic numbers and provided on separate sheets together with relevant captions. In one table the column number is maximum 13 if possible. One column should not contain more than five characters.

Mathematical formulas and *symbols:* non-Latin letters and hand-written marks should be explained by making marginal notes in pencil.

The final text should be submitted both in manuscript form and on *diskette.* Use standard 3.5" or 5.25" DOS formatted diskettes for this purpose. The following word processors are supported: WordPerfect 5.1, WordPerfect for Windows 5.1, Microsoft Word 5.5, Microsoft Word for Windows 2.0. In all other cases the preferred text format is ASCII.

* * *

Authors receive 30 *reprints* free of charge. Additional reprints may be ordered at the authors' expense when sending back the proofs to the Editorial Office.

Published by the Hungarian Meteorological Service

Budapest, Hungary

INDEX: 26 361

HU ISSN 0324-6329